DNAJB1-PRKACA fusion protein-regulated LINC00473 promotes tumor growth and alters mitochondrial fitness in fibrolamellar carcinoma

Rosanna K. Ma[1], Pei-Yin Tsai[2], Alaa R. Farghli[1], Alexandria Shumway[1], Matt Kanke[1], John D. Gordan[3], Taranjit S. Gujral[4], Khashayar Vakili[5], Manabu Nukaya[6], Leila Noetzli[7], Sean Ronnekleiv-Kelly[6], Wendy Broom[7], Joeva Barrow[2], and Praveen Sethupathy[1]

[1] *Department of Biomedical Sciences, College of Veterinary Medicine, Cornell University, Ithaca, New York.*
[2] *Division of Nutritional Sciences, Cornell University, Ithaca, New York.*
[3] *Division of Hematology/Oncology, Helen Diller Family Comprehensive Cancer Center, UCSF, San Francisco, California.*
[4] *Human Biology Division, Fred Hutchinson Cancer Center, Seattle, Washington.*
[5] *Department of Surgery, Boston Children's Hospital, Boston, Massachusetts.*
[6] *Department of Surgery, Division of Surgical Oncology, University of Wisconsin School of Medicine and Public Health, Madison, Wisconsin.*
[7] *Alnylam Pharmaceuticals, Cambridge, Massachusetts.*

Corresponding Author: Praveen Sethupathy, Cornell University, Veterinary Research Tower T7 006D, Ithaca, NY 14853. Phone: 607-253-4347; Fax: 607-253-4447; E-mail: pr46@cornell.edu

Summary

Fibrolamellar carcinoma (FLC) is a rare liver cancer that disproportionately affects adolescents and young adults. Currently, no standard of care is available and there remains a dire need for new therapeutics. Most patients harbor the fusion oncogene *DNAJB1-PRKACA* (DP fusion), but clinical inhibitors are not yet developed and it is critical to identify downstream mediators of FLC pathogenesis. Here, we identify long non-coding RNA LINC00473 among the most highly upregulated genes in FLC tumors and determine that it is strongly suppressed by RNAi-mediated inhibition of the DP fusion in FLC tumor epithelial cells. We show by loss- and gain-of-function studies that LINC00473 suppresses apoptosis, increases the expression of FLC marker genes, and promotes FLC growth in cell-based and *in vivo* models of disease. Mechanistically, LINC00473 plays an important role in promoting glycolysis and altering mitochondrial activity. Specifically, LINC00473 knockdown leads to increased spare respiratory capacity, an indicator of mitochondrial fitness. Overall, we propose that LINC00473 could be a viable target for this devastating disease.

Highlights

Fibrolamellar carcinoma (FLC) is a lethal liver cancer lacking effective therapeutic options. Ma et al. demonstrate that primate-specific RNA LINC00473 is enriched in tumor epithelial cells and functions to promote FLC growth and dysregulate cellular energetics, unveiling an important mechanism downstream of the fusion oncogene, DNAJB1-PRKACA, in FLC pathogenesis.

In Brief

- LINC00473 is consistently elevated in primary FLC tumor tissue from different patient cohorts and in multiple disease models.
- DP fusion, the signature oncoprotein of FLC, drives LINC00473 expression.
- LINC00473 promotes FLC growth via anti-apoptotic function.
- LINC00473 modulates FLC energetics by promoting glycolysis and altering mitochondrial fitness.

Keywords: LINC00473, fibrolamellar, mitochondria, glycolysis, apoptosis

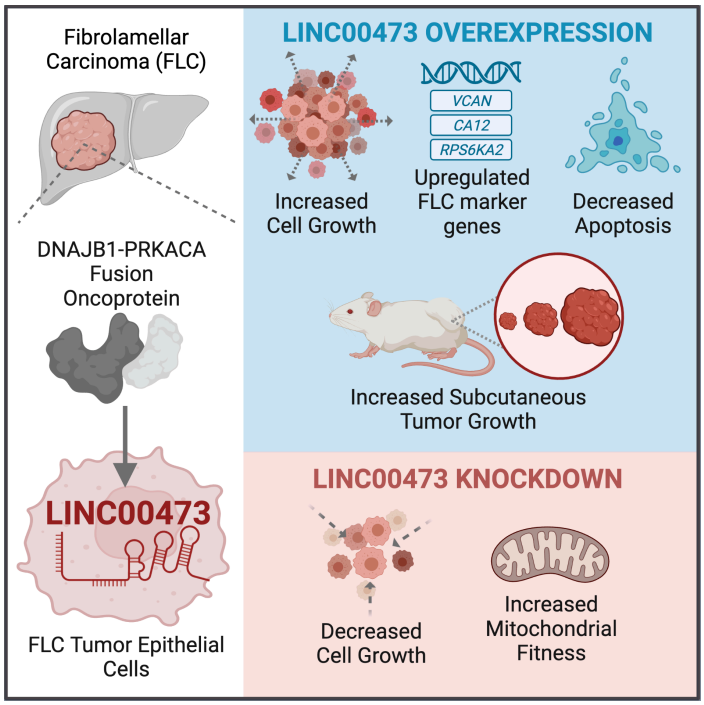

Introduction

Fibrolamellar carcinoma (FLC) is a rare and aggressive type of liver cancer that disproportionately affects young adults, with a median age of onset at 22 years[1–6]. FLC constitutes ~13% of liver cancers for patients less than 40 years old[3]. Unlike adult-onset liver cancers, FLC presents with vague symptoms, lacks diagnostic serum biomarkers, and is not associated with known liver cancer risk factors[4–7]. Surgical resection remains the only curative treatment approach; however, the majority of diagnoses occur at advanced metastatic stages of disease, leading to surgical ineligibility, high rates of recurrence, and poor survival[8–10]. The dire need for therapeutics is underscored by how FLC tumors are resistant to drugs currently used to treat other liver cancers[2,5,8–10].

At the genomic level, FLC tumors are characterized by a somatic, heterozygous ~400kb deletion on chromosome 19 that results in a fusion gene called *DNAJB1-PRKACA* (DP fusion)[11,12]. The fusion consists of the chaperone-binding domain of heat shock protein 40 (DNAJB1) and the alpha isoform of the catalytic subunit of protein kinase A (PRKACA). The DP fusion is detected in the vast majority of patient tumors and is widely appreciated as the main FLC driver gene[4,13]. Functionally, the DP fusion is sufficient for initiating tumor formation in mice[14,15] and is also likely important for tumor maintenance[16], but specific pharmacological targeting of the oncoprotein has proved challenging[17–19]. Therefore, it is critical to identify and target candidate downstream effectors that drive FLC development and progression. Genome-scale studies of FLC tumors have identified many dysregulated genes that are hypothesized to be sensitive to DP fusion activity, and these merit deeper investigation as alternative therapeutic targets[20–28].

Long noncoding RNAs (lncRNAs) are critical regulators of gene expression at the transcriptional and post-transcriptional levels[29–32]. Defined as transcripts over 200 nucleotides in length with little to no protein-coding potential, lncRNAs are frequently expressed in a tissue- and disease-specific manner[33,34]. Functionally, lncRNAs exhibit highly specific cell-type and subcellular expression patterns and bind to proteins, as well as chromatin and RNA, to mediate gene regulation[29,32–37]. Emerging evidence shows that some lncRNAs are abnormally expressed in tumors and play important roles in cell cycle progression, uncontrolled proliferation, anti-apoptosis, dysregulated metabolism and metastasis[38–46]. This suggests that lncRNAs are both targets and regulators of cancer-specific transcriptional programs.

LINC00473 is a putative oncogenic lncRNA in a few cancer types and is part of a reported gene signature of FLC[21,47–50]. The introduction of *DNAJB1-PRKACA* into human embryonic kidney HEK293 cells led to potent LINC00473 upregulation[51]. Furthermore, FLC tumor-specific enhancers adjacent to LINC00473 are highly enriched in cAMP response binding protein (CREB) binding motifs[52]. This is intriguing because CREB is a critical mediator of PKA signaling and has been suggested to regulate LINC00473 in normal physiological and disease settings[47,48,53–56]. However, the functional significance of LINC00473 in FLC is unknown.

To bridge this knowledge gap, we evaluated the function of LINC00473 in FLC progression using genome-wide analyses combined with functional molecular studies in both cell-based and *in vivo* mouse models. We show that the DP fusion induces LINC00473 expression in tumor epithelial cells to facilitate FLC growth and survival. Our findings implicate a role for LINC00473 in altering mitochondrial activity that may influence pro-tumorigenic cancer cell energetics in FLC. This body of work establishes LINC00473 as one of the most well-characterized FLC marker genes to date. We hypothesize that LINC00473 is a promising diagnostic marker of DP fusion activity and a candidate therapeutic target for FLC.

Results

LINC00473 represents a distinct transcription unit in FLC tumors

In recent years, the LINC00473 locus has been subject to variable annotation across different databases. For example, according to some annotation libraries, the LINC00473 transcript is collapsed into an isoform of a nearby protein-coding gene, *PDE10A*. However, a recent comparative genomic analysis clearly demonstrated that the expression of LINC00473 is driven independently from PDE10A in human neurons derived from induced pluripotent stem cells. The same study confirmed that LINC00473 is present only in higher primates[54]. Several reports have demonstrated that LINC00473 has limited coding potential and showed that any role of a putative protein from this locus is likely negligible[47,54]. Additionally, others have observed that *PDE10A* was not altered in expression upon LINC00473 modulation in human endometrial stromal cells and adipocytes[53,57]. Taken together, these findings strongly indicate that LINC00473 is an independent long, non-coding RNA (lncRNA).

To corroborate this result in the context of FLC tumors, we sought to more directly evaluate the transcriptional activity at the LINC00473 locus using our previously published chromatin run-on sequencing (ChRO-seq) data[52]. ChRO-seq enables the genome-wide detection of nascent transcription[58]. In FLC tumors, we observed very high levels of transcription on the minus strand within the ~49kb and ~63kb windows that mark the gene bodies of LINC00473 variants 1 and 2, respectively (Supplementary Figure 1A). Importantly, transcriptional activity was markedly diminished in the ~250kb gap between the annotated LINC00473 locus and the RefSeq annotation for *PDE10A* (Supplementary Figure 1A). These data confirm that LINC00473 transcription is separate from *PDE10A* and that it is a lncRNA that merits further analysis in FLC.

RNA-seq on an expanded number of primary patient samples reveal LINC00473 as a top up-regulated gene in FLC

To examine differentially expressed genes in FLC, we performed RNA-seq on an expanded set (Cohort 1) of FLC patient tumors (n = 35) and matched non-malignant liver (NML, n = 10) from the Fibrolamellar Cancer Foundation biobank, and confirmed *DNAJB1-PRKACA* (DP fusion) expression in all tumor samples. Our analysis identified LINC00473 as one of the top-most significantly upregulated genes in FLC compared to NML (fold-change > 25, Figure 1A), though there is some variance of expression values across patients (Figure 1B).

We then restricted the analysis to only patient-matched FLC and NML samples in an independent cohort from the Fred Hutchinson Cancer Center (Figure 1C, n = 5), as well as in a subset of Cohort 1 (Figure 1D, n = 9; Supplementary Figure 1B) and confirmed that LINC00473 is indeed significantly elevated in FLC (fold-change > 50). This finding was further validated by RT-qPCR for both isoforms of LINC00473 (TV1, TV2) in a subset of patient-matched samples (Figure 1E, n = 7; Supplementary Figure 1C). A direct comparison of DP fusion and LINC00473 expression levels in FLC tumors indicated a highly significant correlation between these genes (Figure 1F, n = 12).

We then assayed several patient-derived models of FLC, notably patient-derived xenograft (PDX) tissue as well as an FLC cell line established from this PDX, and found that DP fusion and LINC00473 are concordantly elevated (Figure 1G). We also observed dramatic upregulation of both TV1 and TV2 isoforms of LINC00473 in HepG2 cells (Figure 1H) and HEK293 cells (Supplementary Figure 1C) in which the ~400kb heterozygous deletion was induced by CRISPR-Cas9 to generate the DP fusion (we refer to these as HepG2-DP and HEK293-DP, respectively). Together, these data demonstrate that LINC00473 is consistently and robustly elevated in primary tumor tissue and multiple models of FLC.

LINC00473 is enriched in FLC tumor epithelial cells

Despite the clear upregulation of LINC00473 in FLC revealed by bulk tissue analysis, it is not known what cell type(s) within the tumor drive this signal. To address this knowledge gap, we first analyzed our recently published single-nucleus ATAC-seq data on one matched set of FLC primary tumor, metastatic tumor and NML tissue[59]. By examining open chromatin signal on a genome-wide scale, we were able to infer active transcription at gene loci with single nucleus resolution. Our analysis revealed 8 distinct clusters that were subsequently assigned specific cell types using established marker genes of liver-resident cells (Supplementary Figure 2A). Next, we focused on the gene activity

at the LINC00473 locus and determined that it is essentially restricted to FLC tumor epithelial cells (Supplementary Figure 2B-D). Further, we examined the cellular localization pattern of LINC00473 by performing subcellular fractionation followed by RT-qPCR and found that the RNA is enriched in the nucleus, with modest cytoplasmic localization, in FLC cells (Supplementary Figure 2E).

Silencing of the DP fusion leads to LINC00473 suppression

Although it has been shown that LINC00473 expression is sensitive to PKA activity in HEK293-DP cells, this has not been investigated in the context of patient-derived FLC cells[51]. To test this, we performed siRNA-mediated knockdown of PRKACA in FLC cells generated from PDX tumors and confirmed significant suppression of both isoforms of LINC00473, as well as the DP fusion (Figure 2A).

Next, we sought to examine if LINC00473 is also suppressed by the knockdown of the DP fusion specifically. To address this question, we designed three N-acetylgalactosamine (GalNAc)-conjugated siRNAs targeting the fusion junction of *DNAJB1-PRKACA* to specifically suppress the fusion oncogene. We also designed a luciferase-targeting siRNA (siLuc) as negative control. Upon Lipofectamine-mediated transfection of the three DP fusion-targeted siRNAs (siDP#1-3) in FLC cells, we observed robust suppression of the DP oncogene and both isoforms of LINC00473, with the strongest gene silencing mediated by siDP#2 (Figure 2B).

Lipid-based reagents for transfection can damage or influence cells in unpredictable ways and are also not tractable for in vivo delivery. To circumvent this issue, we sought to evaluate gene silencing in FLC cells through transfection-free uptake of siRNAs. We tested several siRNA delivery systems including encapsulation in lipid nanoparticles (LNPs) or conjugation with GalNAc, 2'-O-hexadecyl (C16), or cholesterol. As a proof-of-concept, we targeted *CTNNB1*, which is expressed in FLC cells, using a siRNA sequence previously shown to drive potent and specific gene knockdown. We discovered that, among the methods tested, LNP encapsulation was the most effective delivery method in FLC cells (Figure 2C, D). Notably, we found >90% reduction in gene expression at concentrations as low as 12.5nM. Interestingly, treatments at 5- and 25-fold higher concentrations did not improve gene silencing efficacy, suggesting that a concentration in the range of 2.5nM - 12.5nM is likely sufficient for gene knockdown (Figure 2D, Supplementary Figure 3A-D). Together, these data demonstrated that siDP#2 (and to a slightly lesser extent, siDP#1) exhibited strong DP fusion silencing and that LNP encapsulation yielded efficient siRNA free uptake in FLC cells.

We next tested whether LNP-mediated delivery of siDP#1 or siDP#2 could achieve potent and specific knockdown of DP fusion in FLC cells. We encapsulated siDP#1, siDP#2, or siLuc control, in LNPs and subsequently treated FLC cells at 5nM. Subsequent western blots were performed using an antibody that binds to the carboxyl terminus of wild-type PRKACA (WT PKA) and detects both native PKA and DP fusion protein. Consistent with previous reports, the major form of the DP fusion was detected at 48kDa[11]. In contrast, the larger band at 51kDa corresponds to the minority oncoprotein, which has been shown previously to be present in the PDX model used to derive the FLC cell line[11,60]. We observed a significant reduction in DP fusion protein expression in response to siDP-LNPs (Figure 2E, F). Although we also observed decreased WT PKA protein abundance, the suppression of DP fusion protein was ~3-fold greater by comparison (Figure 2F). WT DNAJB1 levels were unaltered after treatment (Figure 2F, Supplementary Figure 3E). Importantly, we found that knockdown of the DP fusion by siDP-LNP led to a marked downregulation of LINC00473 and other FLC marker genes (Figure 2G, Supplementary Figure 3F). Together, we demonstrate that a siRNA-LNP approach leads to potent silencing of the DP fusion at the RNA and protein level, as well as robust LINC00473 suppression. These observations provide strong evidence that LINC00473 expression is driven by the DP fusion in FLC.

FLC cell growth is altered following LINC00473 knockdown or overexpression

To interrogate the function of LINC00473 in FLC, we developed complementary gene knockdown and overexpression approaches using lentiviral integration of short hairpin RNAs (shRNAs) or cDNA to enable stable gene modulation in FLC cells. For gene knockdown, two distinct LINC00473-targeting shRNAs (sh473-2, sh473-4) that were previously reported to strongly downregulate LINC00473 TV1 and non-targeting control (shCtl) were cloned into lentiviral plasmids and subsequently transduced in FLC cells[47]. Following antibiotic selection, the majority of transduced FLC cells were predicted to

express a single copy of shRNA to mitigate off-target effects. Using RT-qPCR to query gene silencing, we showed that sh473-2 and sh473-4 yield efficient gene knockdown by 80% and 50%, respectively (Figure 3A). Interestingly, although the shRNAs were originally designed to target LINC00473 TV1, the expression of the second isoform was also modestly decreased upon treatment (Figure 3B). For gene upregulation, the cDNA sequence of LINC00473 TV1 was cloned into a LeGO-lnc lentiviral vector (LeGO-473ox). We followed a similar method of transduction as with the shRNA integration, resulting in a dramatic 85-fold increase in gene expression levels compared to empty LeGO-lnc vector control (LeGO-Ctl) (Figure 3C, Supplementary Figure 4A).

We first assessed the effect of LINC00473 on FLC cell growth using our polyclonal knockdown and overexpression cell lines. By examining cell counts over 5 days, we found that the stable downregulation of LINC00473 using sh473-2 or sh473-4 significantly decreased cell growth across two independent trials (Figure 3D). Concordantly, increased cell growth was observed in polyclonal FLC cells expressing elevated levels of LINC00473 relative to LeGO-Ctl (Figure 3E). To mitigate the effects of genetic drift in cell culture, we performed limiting dilutions on our engineered polyclonal cells to develop several independent monoclonal cell lines. As expected, monoclonal cells displayed a range of LINC00473 downregulation and overexpression as determined by RT-qPCR (Supplementary Figure 4B, C). To confirm that LINC00473 regulates FLC cell growth, we selected three monoclones from each group for cell growth quantification: sh473-2 (clones A3, A4, A6), sh473-4 (clones B2, B3, B4), shCtl (clones C2, C5 C6), LeGO-473ox (clones D3, D4, D6), and LeGO-Ctl (clones E1, E5, E6). In line with our prior data, monoclonal cell growth decreased under conditions of LINC00473 suppression (Figure 3F), which is validated in similarly engineered HEK293-DP monoclones with shRNA integration (Supplementary Figure 4D-F), and increased levels of LINC00473 led to enhanced cell growth (Figure 3G).

To further validate the role of LINC00473 in regulating cell growth in FLC, we next examined the effects of LINC00473 inhibition and upregulation on anchorage-independent colony formation. Monoclonal cell lines harboring LINC00473 knockdown (clone A3) or overexpression (clone D3), as well as the corresponding controls (clones C2, E6, respectively), were analyzed for colony growth at 14 days after seeding. Consistent with our cell growth data, FLC cells exhibited drastically decreased colony expansion upon LINC00473 silencing (Figure 3H), and elevated levels of LINC00473 resulted in significantly greater colony growth (Figure 3I). Taken together, these data confirm that LINC00473 is a key regulator of cell growth in FLC.

LINC00473 increases FLC cell survival by suppressing apoptosis

To determine which genes and pathways are most altered in response to perturbation of LINC00473, we performed RNA-seq on multiple independent monoclonal cell lines with LINC00473 overexpression (LeGO-473ox clones D3, D4) or empty vector control (LeGO-Ctl clones E5, E6). Our differential gene expression analysis identified 1403 up-regulated genes and 1374 down-regulated genes in LeGO-473ox cells compared to LeGO-Ctl controls. As expected, we found that LINC00473 itself is one of the top-most elevated genes in LeGO-473ox (Figure 4A). Principal component analysis (PCA) showed stratification of samples by condition based on gene expression profiles (Figure 4B). Furthermore, unsupervised hierarchical clustering analysis confirmed that LeGO-473ox clones segregated completely from LeGO-Ctl control clones (Figure 4C).

We proceeded to evaluate the expression of key FLC marker genes known to be highly elevated in primary tumors, including *CA12*, *VCAN*, *OAT*, *TESC*, and *RPS6KA2*. We confirmed that the majority of the queried genes were robustly increased in expression in FLC cells in which LINC00473 was overexpressed (Figure 4D, Supplementary Figure 5A), suggesting that LINC00473 may play a role in regulating the expression of key FLC-associated genes.

Next, we performed pathway enrichment analysis using ENRICHR[61]. Strikingly, genes upregulated by LINC00473 were most highly enriched in metabolic pathways including glycolysis (Figure 4E), pentose phosphate pathway, galactose metabolism (Supplementary Figure 5B), and mitochondrial respiratory chain dysfunction (Supplementary Figure 5B). Additionally, cancer metabolism-related genes including *PFKM*, *IDH3G*, *PYCR1*, and *BCAT1* were strongly elevated in expression in response to increased LINC00473 levels (Figure 4E). We also found that genes downregulated by LINC00473 were most enriched in apoptosis pathways (Figure 4F, Supplementary Figure 5C). Furthermore,

MSigDB Hallmark pathway analysis ranked apoptosis as the 6th most enriched pathway (Supplementary Figure 5C), and genes that encode for pro-apoptotic proteins, such as *BCL2, TRIB3, KLF10*, and *GADD45B* were markedly suppressed in the context of LINC00473 upregulation (Figure 4F). Together, these data implicate LINC00473 as a regulator of metabolism and a suppressor of apoptotic pathways in FLC cells.

To investigate whether LINC00473 increases FLC cell growth by altering the rate of cell proliferation, cell death, or both, we performed EdU incorporation assays and TUNEL assays in FLC monoclones harboring sh473-mediated LINC00473 knockdown or shCtl, and LeGO-473ox-driven LINC00473 overexpression or LeGO-Ctl. EdU incorporation rates were not indicative of notable differences in cell proliferation across groups (Figure 4G). In contrast, TUNEL staining revealed a striking reduction of cell death in the context of LINC00473 over-expression and a significant increase in cell death upon LINC00473 knockdown (Figure 4H). Thus, decreased apoptosis in LINC00473-overexpressing FLC cells likely underlies their elevated growth relative to control cell lines. These findings further implicate LINC00473 as a regulator of FLC cell growth that functions, in part, to suppress apoptotic pathways.

Piqued by the recurrent theme of metabolic pathways among the genes upregulated by LINC00473-overexpressing cells, we investigated which of these genes are also altered in FLC tumors. By comparing the genes that are significantly elevated in FLC tumors relative to NML (n = 1667), and in LeGO-473ox cells relative to control (n = 1403), we found a significant number of overlapping genes (n = 188, $p=4.81 \times 10^{-20}$, Figure 4I). We determined that these 188 genes are over-represented in pathways linked to metabolic effects of oncogenes, cancer metabolic reprogramming, glutamine in cancer metabolism, and proline metabolism (Figure 4I, Supplementary Figure 5D). Remarkably, energy metabolism-related genes such as *BCAT1*, *CTH*, *PFKM*, *PRODH*, *PYCR1*, and *SLC7A11* stood out among the overlapping genes as the most highly upregulated in both FLC tumors and in FLC cells with increased LINC00473 expression.

A parallel analysis was performed on the genes most significantly down-regulated in both FLC tumors and LeGO-473ox cells. This examination revealed an intersection of 91 genes, including *FOS*, *GADD45A/B*, *KLF10/11*, and *TRIB3*, which are involved in p53 signaling and apoptosis (Figure 4J, Supplementary Figure 5E). Taken together, these findings strongly suggest that LINC00473 plays a role in dysregulated energetics in FLC and in the suppression of apoptosis in FLC.

LINC00473 functions to increase glycolysis and mitochondrial activity in FLC cancer metabolism

We next explored how LINC00473 regulates cellular energetics in FLC. To investigate this, we performed Seahorse metabolic analyses on FLC monoclones harboring stable LINC00473 knockdown (sh473) and non-targeting control (shCtl) or overexpression (LeGO-473ox) and empty vector control (LeGO-Ctl). This enabled the examination of glycolysis using extracellular acidification rate (ECAR), which monitors changes in pH levels as a readout of lactate production. Several parameters of glucose metabolism are measured as cells respond to a series of compounds that alter glycolytic function. We observed that LINC00473 upregulation led to a marked elevation in glucose utilization, as shown by increased levels of glycolysis and glycolytic capacity in LeGO-473ox cells relative to LeGO-Ctl (Figures 5A, B). In contrast, LINC00473 silencing resulted in a trend toward decreased glycolysis, although the result was not significant (Figures 5C, D).

Next, we investigated the effect of LINC00473 on mitochondrial respiration by quantifying oxygen consumption rate (OCR). By tracking oxygen levels as cells respond to a series of modulators that perturb the electron transport chain, we were able to quantify several parameters of mitochondrial respiration in our knockdown and overexpression FLC cell lines. Spare respiration capacity (SRC) is calculated by subtracting maximum respiration from basal respiration and reveals the adaptability of mitochondria to meet acute energy demands, thereby serving as an indicator of mitochondrial fitness in stress conditions. Importantly, SRC dysregulation is a known cancer cell phenotype and we have observed that SRC is dramatically depleted in FLC cells (personal communication, Donald Long, Jr.). In the context of LINC00473 overexpression, we observed a modest elevation in basal respiration in FLC cells compared to empty vector control (Figure 5E, F). Knockdown of LINC00473 led to a prominent

rescue of SRC (Figure 5G, H). In sum, these data suggest that LINC00473 may increase baseline mitochondrial activity at the cost of reduced mitochondrial fitness in FLC cells.

LINC00473 promotes FLC tumor growth

To investigate if the growth-promoting effect of LINC00473 observed in FLC cells persists in the *in vivo* context, we studied tumor growth progression in a xenograft animal model. We implanted FLC cells with LINC00473 overexpression (LeGO-473ox) or empty vector control (LeGO-Ctl) into mice by subcutaneous injection and quantified relative volume progression in each tumor for 8 days. In line with our *in vitro* data, we observed that LINC00473 induction significantly increases tumor growth rate (Figure 6A, B). Further, we assessed gene expression levels in LINC00473-overexpression tumors and confirmed strong upregulation of LINC00473, as well as unaltered expression of the DP fusion, relative to tumor controls (Figure 6C, Supplementary Figure 6A). Taken together, these results confirm the role of LINC00473 as a regulator of FLC growth *in vivo*. A working model of the role of LINC00473 in FLC is shown in Figure 7.

Discussion

FLC is a rare and aggressive type of liver cancer that often presents at advanced stages owing in part to the lack of diagnostic biomarkers and known risk factors. Faced with a paucity of treatment options, FLC patients suffer from low survival rates. There has been exciting progress over the past decade in the pursuit of driver genes, most notably the identification of the signature *DNAJB1-PRKACA* (DP) fusion oncogene. However, the development of specific inhibitors of the DP fusion remains a challenge and there persists an urgent and unmet need for effective therapies[17,18]. The mechanisms by which the fusion oncogene transforms cells remain poorly understood. To gain deeper insight into FLC molecular etiology, we leveraged multiple genome-scale strategies and functional approaches, which revealed LINC00473 as a critical regulator of FLC phenotypes.

LINC00473 is a primate-specific long-noncoding RNA and its normal functions are poorly understood[54,57]. Earlier reports provided little-to-no support for coding potential at the LINC00473 locus[47]. Pruunsild et al. recently showed that the open reading frame could be translated; however, for various reasons, the authors concluded that the function of the putative protein is likely negligible compared to the lncRNA transcript[54]. In the future, it will be of interest to evaluate whether any small peptides are produced from this locus in FLC tumors.

LINC00473 has been reported in different subcellular compartments in distinct cellular contexts and disease states[54–56]. For instance, in non-small cell lung tumors, Chen et al. found that LINC00473 was primarily nuclear with modest cytoplasmic expression, whereas in adipocytes Tran et al. showed that LINC00473 can localize to the mitochondria[47,57]. Known protein binding partners of LINC00473 are NONO in several cell types as well as PLIN1 in adipocytes[47,48,57]. In normal conditions, LINC00473 exhibits a very restricted pattern of expression across tissues, with the greatest abundance in the ovary, pituitary gland, and fallopian tube[62].

The limited literature on LINC00473 has impeded understanding of its biological role and molecular regulation in disease. However, LINC00473 has been reported to be elevated in several cancer types and described as a predictor of poor prognosis[21,47–50]. For instance, one study identified LINC00473 as a cAMP/CREB target gene required for the growth and survival of non-small cell lung tumors with an inactivating mutation in the tumor suppressor gene *LKB1*[47]. Other reports demonstrated that LINC00473 is downstream of the fusion oncoprotein CRTC1-MAML2 in mucoepidermoid carcinoma, and that the deletion of CRTC2/3 leads to decreased levels of LINC00473[48,63]. In contrast, LINC00473 was discovered to be transcriptionally silenced due to promoter hypermethylation in colorectal cancer and was suppressed in osteosarcoma cells by the direct binding of ZBTB7A (encoding Pokemon) to the LINC00473 promoter[50,64].

LINC00473 has been implicated as a target of cAMP/CREB signaling beyond malignant contexts as well. For instance, Liang et al. uncovered that LINC00473 mediates decidualization of human endometrial cells in response to cAMP signaling[53]. Others found that the ectopic expression of LINC00473 in mouse neurons leads to the upregulation of CREB target genes *Bdnf* and *Rheb*, which participate in a positive feedback loop to maintain CREB signaling[54]. In this study, we determined that in FLC, LINC00473 is responsive to the inhibition of the DP fusion and wild-type PKA. Also, our previous analyses revealed that a subset of cholangiocarcinoma tumors characterized by the *ATP1B1-PRKACA* fusion, which retains the same *PRKACA* exons as the DP fusion, express elevated levels of LINC00473[52]. The strong connection between aberrant PKA signaling and LINC00473 expression is likely mediated by CREB transcription factor activity. Our group previously reported that the LINC00473 locus is associated with a FLC tumor-specific super-enhancer enriched for CREB-binding motifs and we demonstrate in this study that its overexpression leads to the upregulation of CREB target genes[52]. Taken together, the findings point to an important role for aberrant PKA signaling, including the DP fusion, in driving LINC00473 expression mediated in part by CRTC/CREB transcription. Previous investigations have shown that PKA regulates CRTC/CREB activity via control of SIK kinases[65–68]. Given that SIK is downstream of LKB1, and that LINC00473 is increased upon LKB1 inactivation, it is possible that SIK is a critical upstream regulator of LINC00473 in FLC[47,69–71]. We propose a model in which DP fusion activity suppresses SIK, which in turn hyperactivates CRTC/CREB and ultimately leads to the aberrant elevation of LINC00473. This model merits further evaluation in future investigations of LINC00473 in FLC.

A major strength of our study is the combination of genome-scale and functional approaches, in patient samples and patient-derived disease models, to interrogate the significance of LINC00473 in FLC. Our analyses on matched patient samples reveal that the expression levels of LINC00473 and the DP fusion are highly correlated in primary tumors and that this coordinate expression is likely restricted to tumor epithelial cells. The latter finding is particularly relevant given that the cell-based disease model in which we evaluate LINC00473 function is comprised primarily of FLC tumor epithelial cells from a patient-derived xenograft.

We highlight the role of LINC00473 in altering glycolysis and mitochondrial fitness in FLC, which is notable given the dearth of knowledge on both LINC00473-driven phenotypes and FLC metabolism. In our lab, we have observed low levels of spare respiratory capacity (SRC) in FLC cells (personal communication, Donald Long, Jr.), suggesting that FLC mitochondria cannot readily adapt to acute energy stressors[72]. In this study, we revealed that LINC00473 is at least partly responsible for the low SRC phenotype in FLC. We also uncovered that LINC00473 increases the expression of genes in metabolic pathways that are activated in FLC, including glutamine metabolism and proline synthesis. PYCR1 confers the final step of proline synthesis and is considered a pro-tumorigenic gene commonly overexpressed in cancers[73]. Studies have demonstrated that increased levels of mitochondrial redox facilitate PYCR1 to drive glutamine flux into proline synthesis[73,74]. Moreover, oxidative stress significantly reduces SRC[75]. Strikingly, our RNA-seq data reveals that PYCR1 is among the most prominently upregulated genes in FLC tumors as well as in LINC00473-overexpressing FLC cells, and is also significantly elevated in LINC00473-induced mouse neurons[54]. It may be the case that LINC00473 sustains high levels of basal respiration and subsequently increases reactive oxygen species abundance, which compromises overall mitochondrial fitness.

A well-established challenge in the FLC field is the scarcity of disease models[4]. For a few years, the only available cell-based model of FLC was the DP fusion-expressing AML12 mouse hepatocyte line[27]. A major limitation of this model for evaluating the primate-specific LINC00473 is its murine origin. In more recent years, at least two other human cancer lines were engineered to express the fusion oncogene, both of which we confirm to exhibit elevated levels of LINC00473[51,76]. While it has been shown that the exogenous introduction of LINC00473 in mouse neurons can modulate synaptic activity, it is unknown whether the transcriptional programs and signaling pathways critical for LINC00473-mediated cancer phenotypes are conserved in non-primate contexts[54,55].

The development of a DNAJB1-PRKACA inhibitor has encountered major challenges due to the inhibition of wild-type PKA, which serves critical roles in maintaining normal physiology in multiple tissues[17–19,77]. Here, we observed that DP fusion-positive FLC cells depend on LINC00473 for cell growth and survival. Given that LINC00473 expression is restricted to few tissue types, we propose that LINC00473 is a candidate target for blocking FLC tumor growth as part of systemic combination therapy. RNAi-based therapies are currently in clinical trials for cancer and other diseases, and additional research may indicate their potential application for lncRNA inhibition[78,79].

A major next step in the examination of LINC00473 pertains to its molecular functions. For example, it would be of interest to interrogate whether LINC00473 localizes to specific areas of chromatin to regulate transcription in a targeted fashion, and what binding partners LINC00473 might have in other compartments of the cell. Another fascinating area that warrants further investigation is the mechanism underlying LINC00473-regulated mitochondrial activity and cellular energetics in FLC. This is particularly interesting due to the growing body of evidence suggesting that altered mitochondrial dynamics are critical to FLC pathology, including aberrant mitochondrial fission[51,80,81].

Together, this study establishes LINC00473 as one of the most well-characterized FLC marker genes to date. We demonstrate that LINC00473 is an important downstream mediator of the DP fusion oncoprotein. Its expression is consistently upregulated in primary FLC tumors and multiple disease models and it is specifically expressed in tumor epithelial cells. Our gain- and loss-of-function approaches identify LINC00473 as a critical regulator of FLC growth and reveal its role in dysregulating energetics in FLC mitochondria. Importantly, our findings strongly support the potential utility of LINC00473 as a biomarker for DP fusion activity for cell-based drug screening efforts, and as a candidate therapeutic target for FLC.

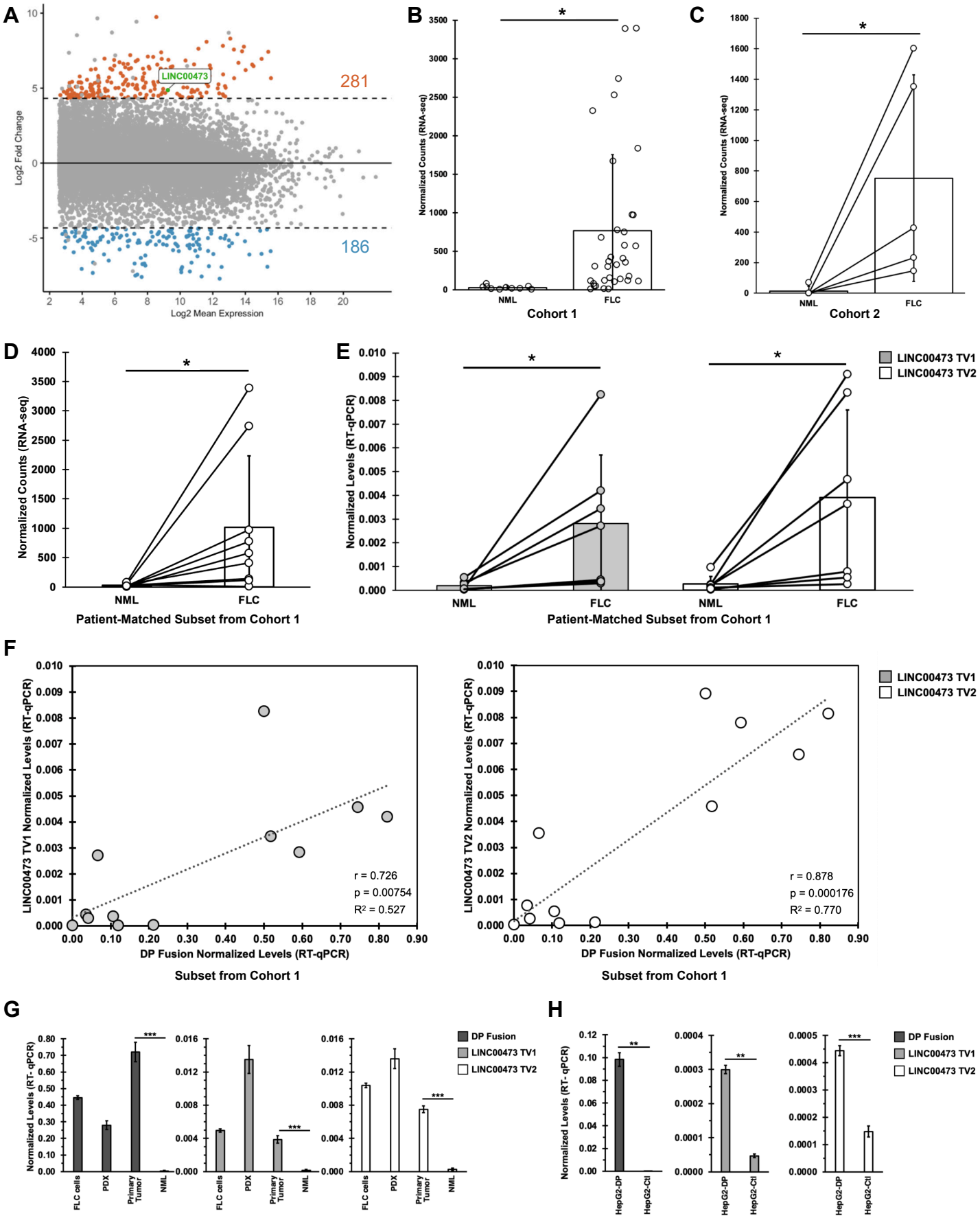

Figure 1: RNA-seq on an expanded number of primary patient samples reveal LINC00473 as a top up-regulated gene in FLC.

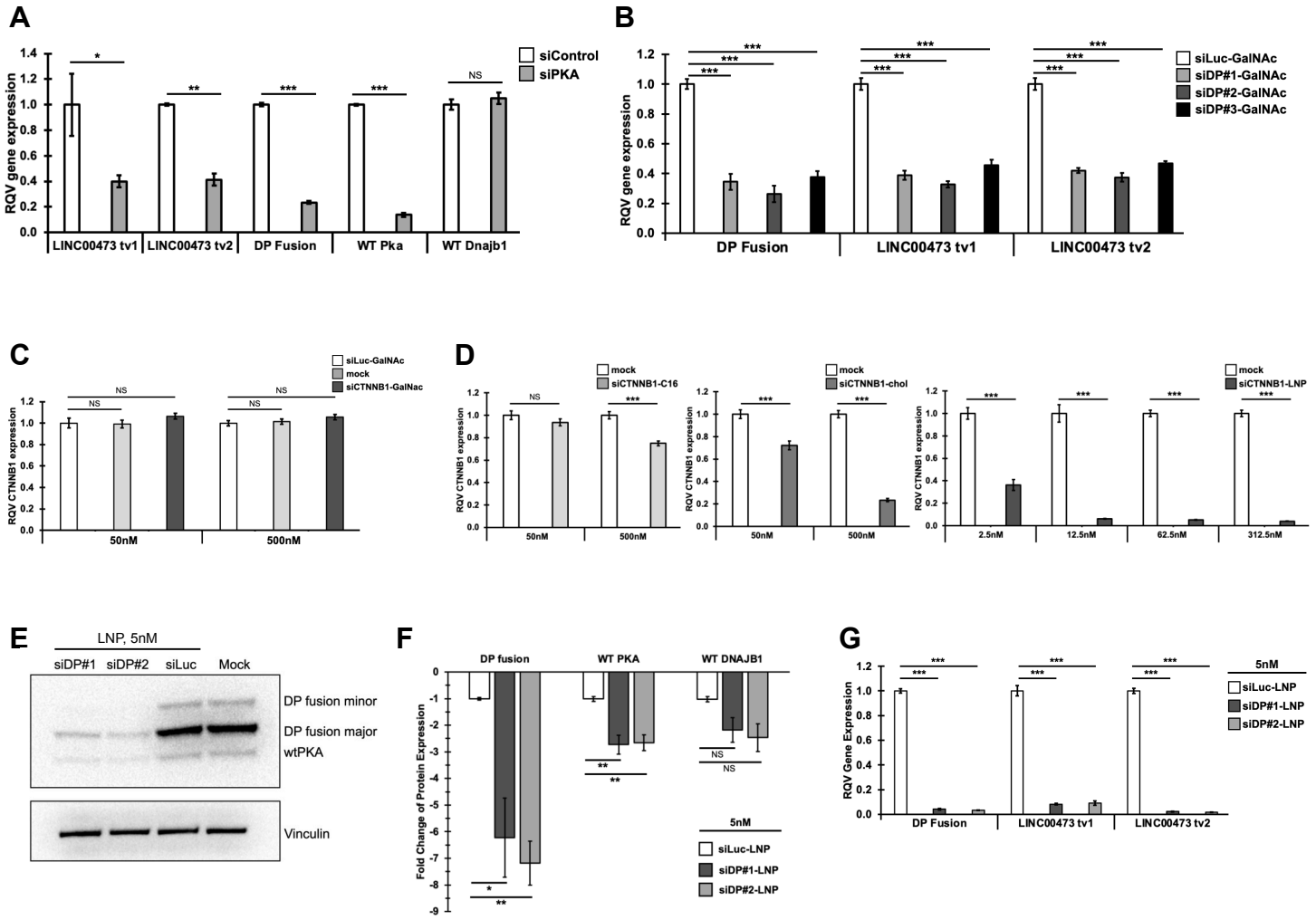

Figure 2. Silencing of the DP fusion leads to the suppression of LINC00473.

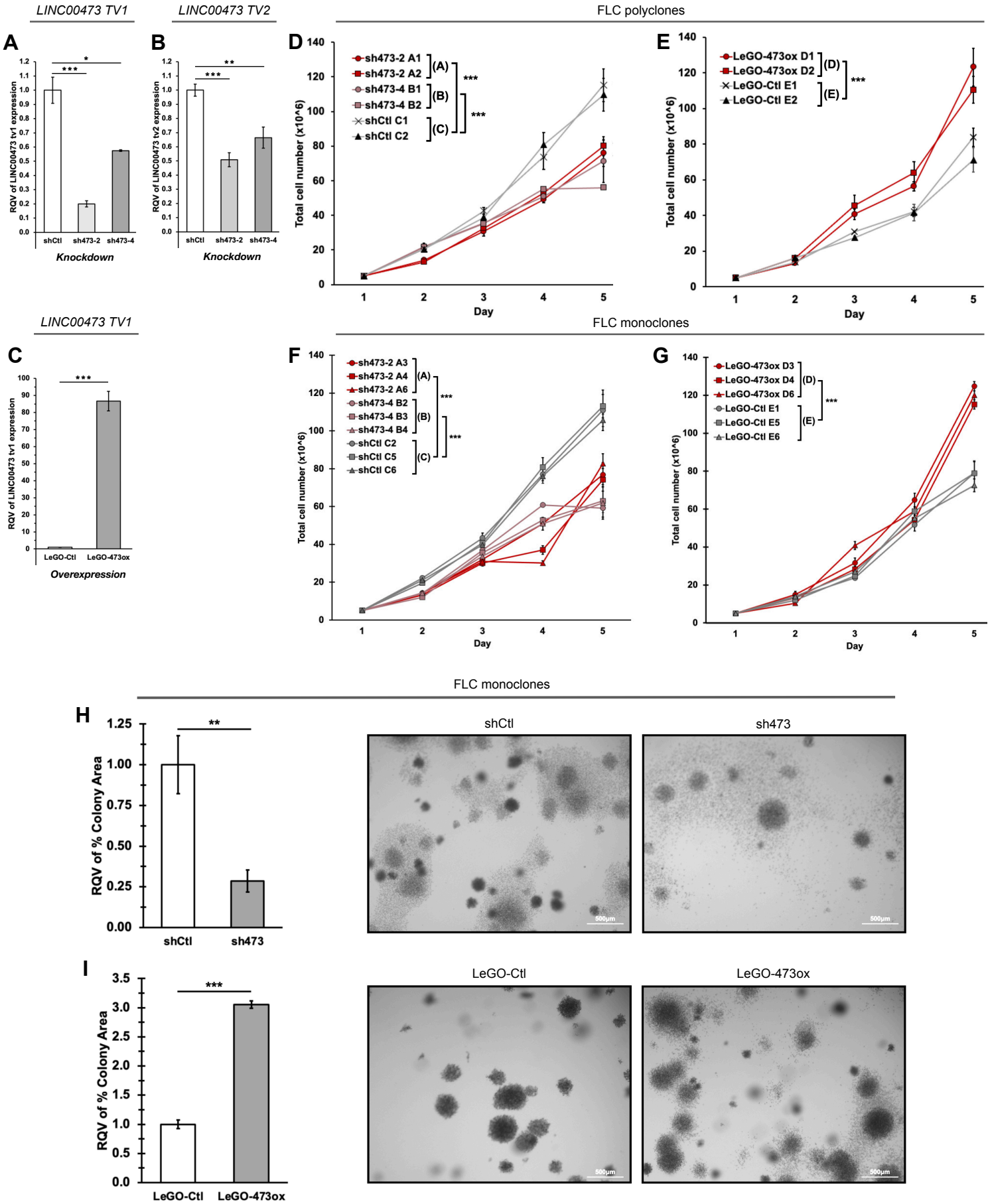

Figure 3. FLC cell growth is altered following LINC00473 knockdown and overexpression.

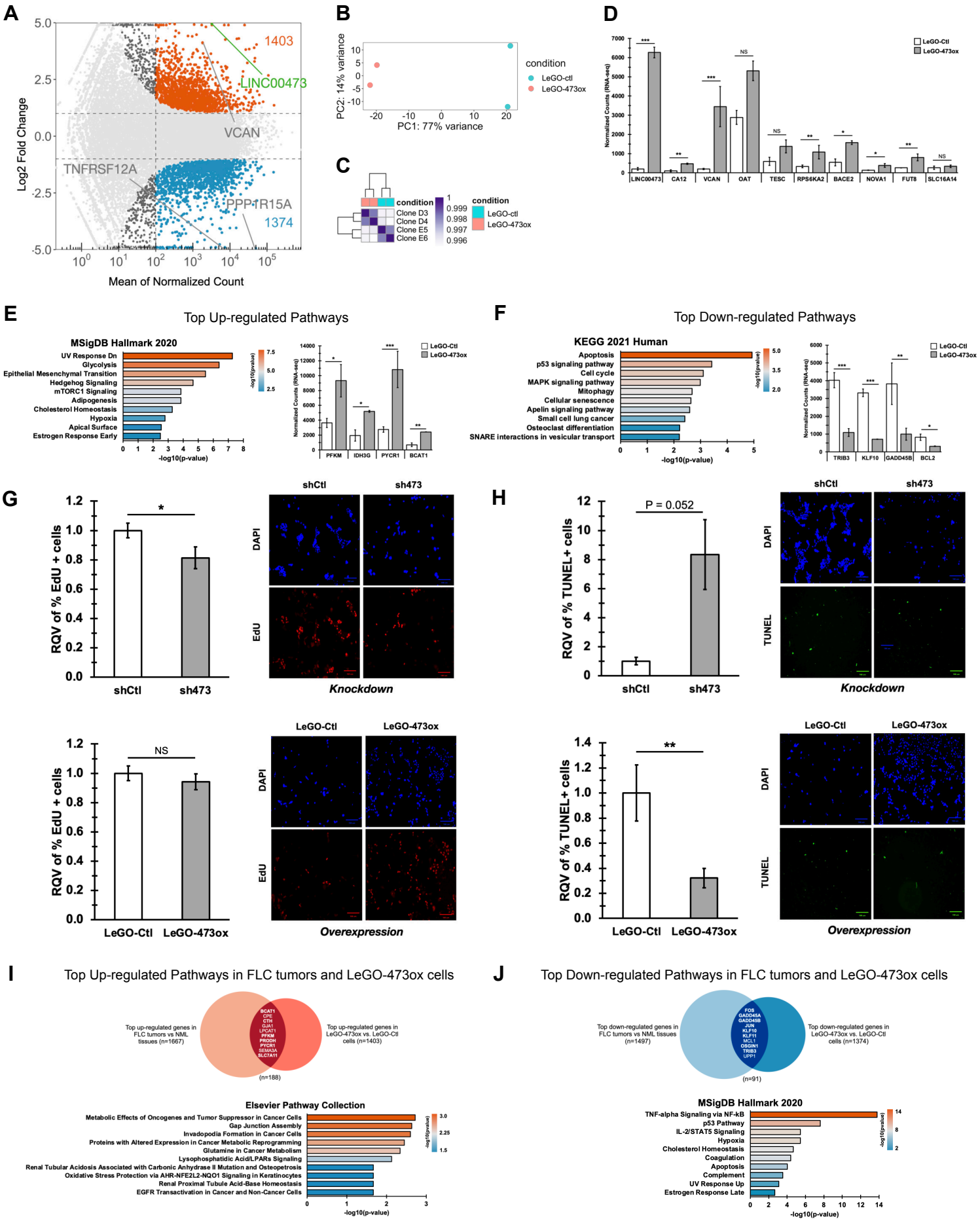

Figure 4: LINC00473 increases FLC cell survival by enhancing apoptosis.

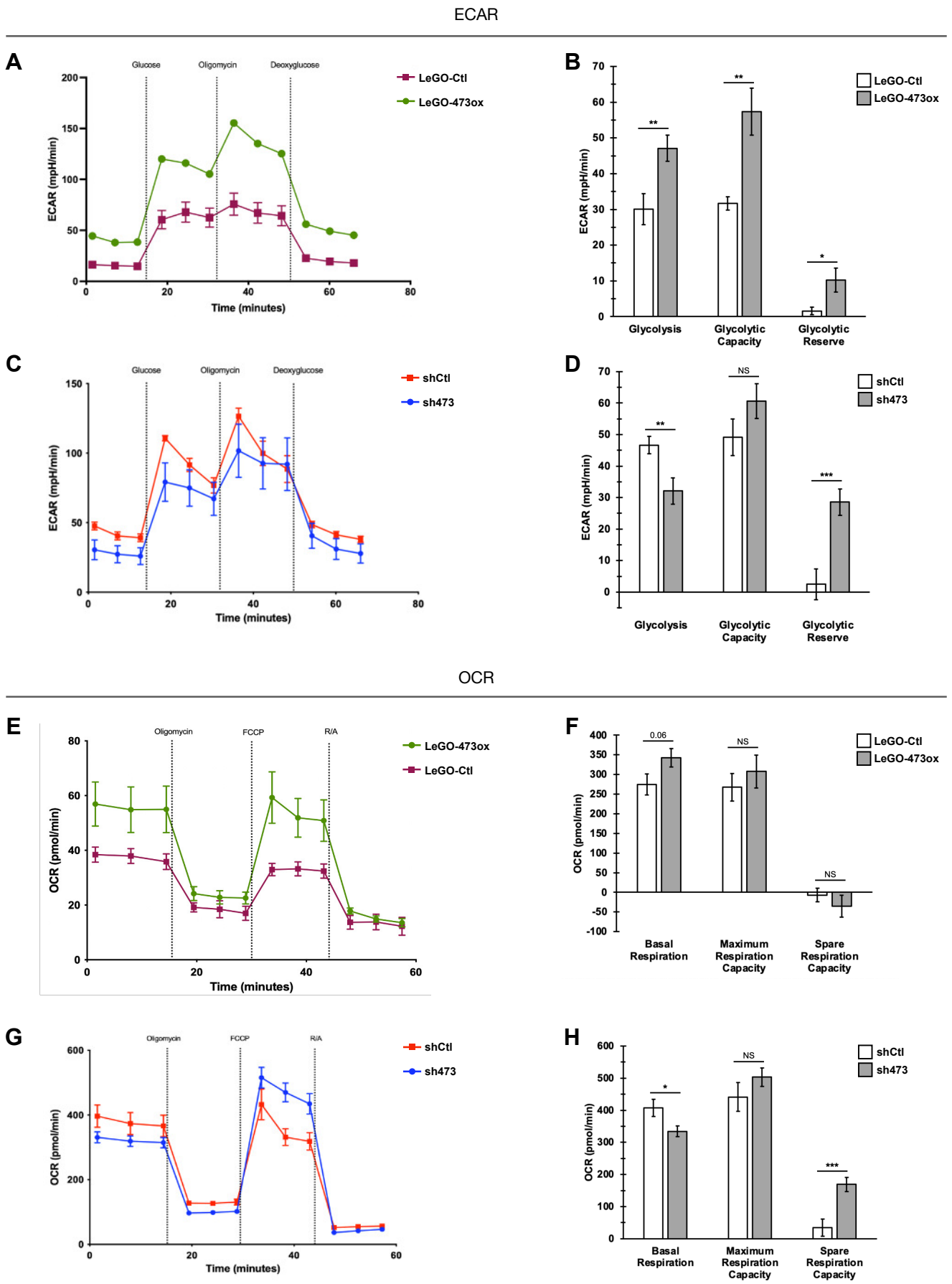

Figure 5: FLC cell growth is altered following LINC00473 knockdown and overexpression.

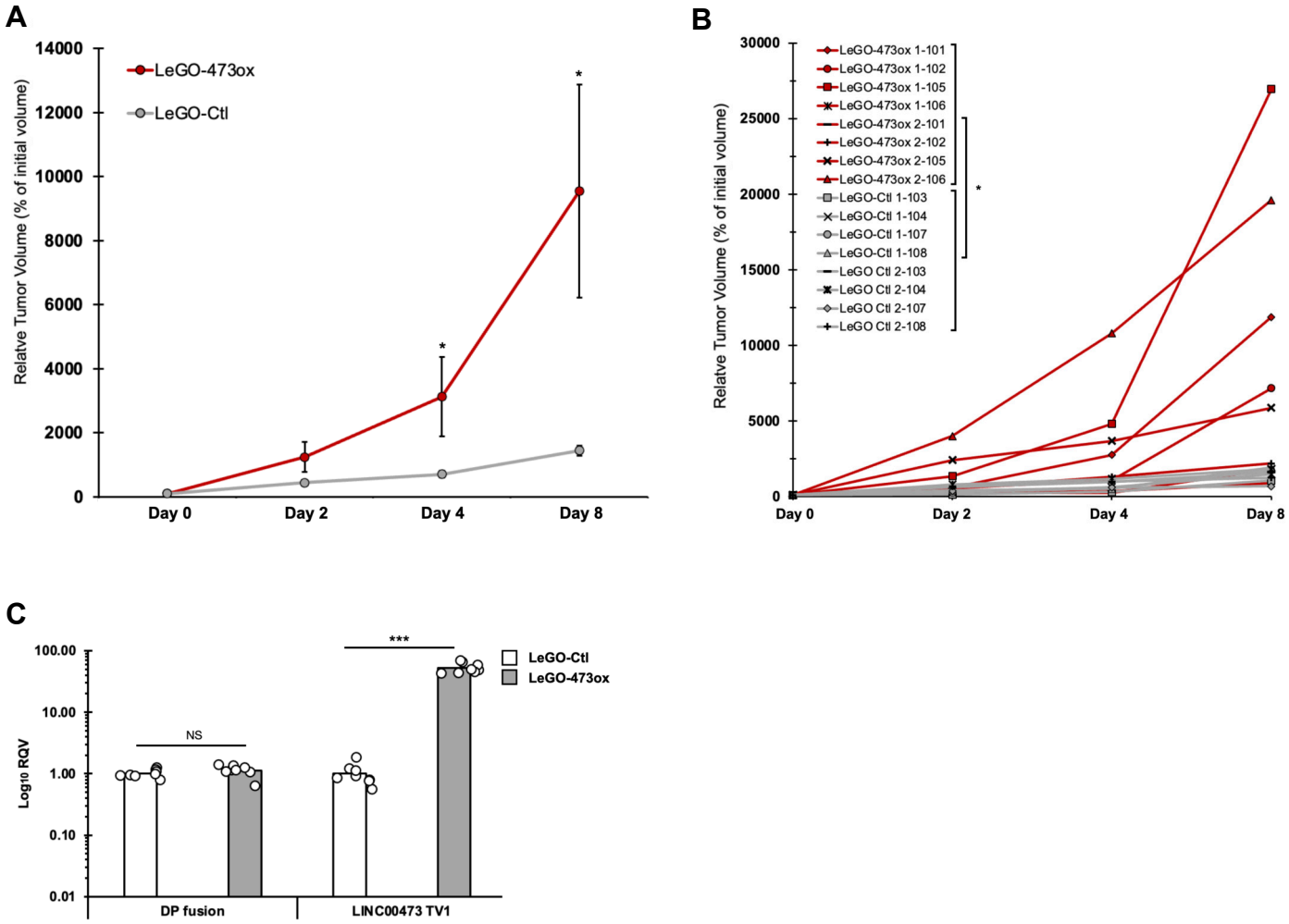

Figure 6. LINC00473 is a regulator of FLC tumor growth in vivo.

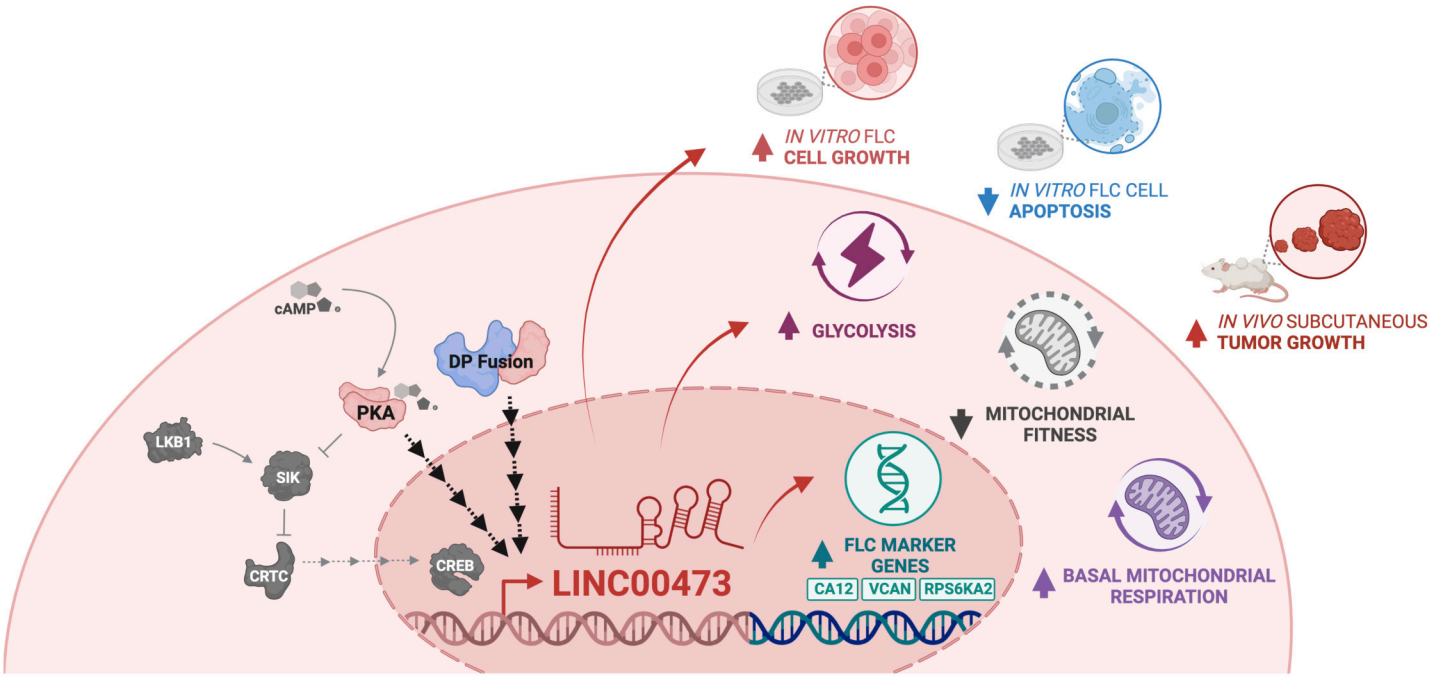

cAMP: cyclic adenosine monophosphate
CREB: camp-response element binding protein
CRTC: cAMP-regulated transcriptional co-activators
LKB1: liver kinase B1
PKA: protein kinase A
SIK: salt inducible kinase

Figure 7. Model of LINC00473 function in FLC.

Figure 1. RNA-seq on an expanded number of primary patient samples reveals LINC00473 as a top up-regulated gene in FLC. (A) MA-plot of genes that are significantly differentially expressed in primary FLC tumors (n = 35) versus non-malignant liver (NML) (n = 10). Genes filtered for expression with base mean > 1000, log2FC > 1 or < -1, and padj < 0.05 (DESeq). Dashed lines represent expression log2 FC of > 4 or < -4. Each dot represents a gene, and significant (padj < 0.05) up- and down-regulated genes are colored orange or blue, respectively. Samples comprise Cohort 1 provided by the Fibrolamellar Cancer Foundation biobank. **(B)** Normalized counts of LINC00473 as determined by RNA-seq using samples in Cohort 1 (10 NML, 35 FLC). Each dot represents a patient sample**. (C)** Normalized counts of LINC00473 expression as determined by RNA-seq using an independent set of patient-matched NML and FLC samples in Cohort 2 (5 NML, 5 FLC). Each dot is a patient sample, and matched NML/FLC samples are indicated with a connecting line. Samples comprise Cohort 2 provided by the Fred Hutchinson Cancer Center**. (D)** Normalized counts of LINC00473 in FLC patient tumors and matched NML in a subset of samples from Cohort 1**. (E)** Normalized levels of LINC00473 TV1 and TV2 as determined by RT-qPCR in patient-matched NML and FLC from Cohort 1 (n = 7 per group). **(F)** Pearson correlation between transcript levels of DP fusion and LINC00473 isoforms TV1 (left) and TV2 (right) in a subset of primary FLC tumors from Cohort 1 (n = 12). Dashed lines represent the fitted linear regression curve. Each dot represents a FLC patient tumor, and identical tumors were assessed for both TV1 and TV2. R^2 and p values are indicated**. (G, H)** Normalized levels of DP fusion transcript and LINC00473 isoforms TV1 and TV2 RNA in multiple models of FLC and matched NML (G), and HepG2-DP cells relative to non-targeting sgRNA control (HepG2-Ctl) (H). n = 3 biological replicates for PDX, primary tumor and NML, and n = 3 technical replicates for FLC cells, HepG2-DP and HepG2-Ctl cells. For gene expression via RT-qPCR in E, F, G, and H, normalized levels represent 2^(-dCt) values using *RPS9* for normalization. Data are represented as mean ± SD. P values are calculated by 2-tailed Student's t-test. *p < 0.05, **p < 0.01, ***p < 0.001.

Figure 2. Silencing of the DP fusion leads to the suppression of LINC00473. (A) Gene expression following transfection of siPKA or non-targeting siRNA negative control (siControl) at 48nM over 72 hours (n = 2 biological replicates)**. (B)** Gene expression from RT-qPCR following lipofectamine-mediated transfection of three independent N-acetylgalactosamine (GalNAc)-conjugated siRNAs targeting the DP fusion (siDP#1-GalNAc, siDP#2-GalNAc, siDP3-GalNAc) and siLuciferase (siLuc-GalNAc) negative control at 50nM over 48 hours. (n = 3)**. (C)** *CTNNB1* gene expression from RT-qPCR following free uptake of siCTNNB1-GalNAc, siLuciferase (siLuc-GalNAc) negative control at 50nM and 500nM, or mock negative control, over 48 hours (n = 3)**. (D)** *CTNNB1* gene expression from RT-qPCR following free uptake of siCTNNB1 conjugated to 2′-O-hexadecyl (C16) or cholesterol (chol), at 50nM or 500nM and mock negative control, or siRNA encapsulated in lipid nanoparticles (LNP) at 2.5nM, 12.5nM, 62.5nM, and 312.5nM, or mock negative control, over 48 hours (n = 3)**. (E)** Representative immunoblot of protein expression of DNAJB1-PRKACA (DP) fusion. DP fusion is detected with a protein kinase A catalytic α subunit (PKA) antibody. WT PKAc, DP fusion major, and DP fusion minor are identified. Lane 1, siDP#1-LNP; Lane 2, siDP#2-LNP; Lane 3, siLuciferase (siLuc-LNP) negative control; Lane 4, mock negative control. siRNA-LNP treatments at 5nM, or mock condition, over 96 hours. following 5nM treatment with siRNA-LNPs or mock condition over 96 hours. Vinculin loading control is shown in the lower panel and run on the same blot (n = 3)**. (F)** Fold change of protein levels in Fig 3E, relative to siLuc negative control (n = 3)**. (G)** Gene expression from RT-qPCR following free uptake of siDP#1-LNP, siDP#2-LNP, and siLuc-LNP at 5nM treatment over 96 hours in FLC cells (n = 3)**.** Data are represented as mean ± SD. P values are calculated by 2-tailed Student's t-test. *p < 0.05, **p < 0.01, ***p < 0.001.

Figure 3. FLC cell growth is altered following LINC00473 knockdown and overexpression. (A, B) LINC00473 TV1 expression from RT-qPCR in FLC polyclonal cells following lentiviral transfection enabling stable gene knockdown using two independent shRNAs (sh473-2, sh473-4) or non-targeting shRNA control (shCtl) (A) or overexpression using cDNA plasmid encoding LINC00473 TV1 (LeGO-473ox) or empty-vector control (LeGO-Ctl) (B). **(C)** Expression of LINC00473 TV2 isoform in FLC polyclonal cells following lentiviral transfection enabling stable gene knockdown using two independent shRNAs (sh473-2, sh473-4) or non-targeting shRNA control (shCtl)**. (D, E)** Cell growth curve of FLC polyclonal cells with stable LINC00473 knockdown (sh473-2, sh473-4) and non-targeting control (shCtl) (D) or overexpression using LINC00473 cDNA (LeGO-473ox) and empty vector control (LeGO-Ctl) (E)**.** Each polyclonal cell line was quantified 2 times across independent passages (A1, B1, C1 from passage 1; A2, B2, C2 from passage 2), and each point is the average cell count of 3 replicates. **(F, G)** Cell growth curve of FLC monoclonal cells with stable LINC00473 knockdown (sh473-2: clones A3, A4, A6; sh473-4: clones B2, B3, B4) and non-targeting control (shCtl: clones C2, C5, C6) (F), or overexpression (LeGO-473ox: clones D3, D4, D6) and empty vector control (LeGO-Ctl: clones E1, E5, E6) (G). Each monoclonal cell line was quantified 2 times across independent passages, and each point is the average cell count of 3 replicates. **(H, I)** Anchorage-independent soft agar colony formation of FLC monoclonal cells expressing stable LINC00473 knockdown (sh473) relative to control (shCtl) (H), and overexpression (LeGO-473ox) relative to control (LeGO-Ctl) (I). Representative images of nitro blue tetrazolium-stained colonies are shown 14 days after seeding from A3, C2, D3 and E6 (2 trials, n = 3 per monoclonal cell line). Scale bars: 500μM. Bar chart data are represented as mean ± SD, n = 3, unless otherwise stated. Statistical testing on cell growth curves was performed using a 2-tailed Student's t-test following area under the curve analysis using the definite integral of each fitted polynomial function. Otherwise, P values are calculated by 2-tailed Student's t-test. *p < 0.05, **p < 0.01, ***p < 0.001.

Figure 4. LINC00473 increases FLC cell survival by enhancing apoptosis. (A) MA plot showing differentially expressed genes in FLC cells that stably overexpress LINC00473 (LeGO-473ox) relative to empty vector control (LeGO-Ctl). Genes filtered for expression with base mean > 100, log2FC > 0.5 and padj < 0.05 (DESeq). Dashed lines represent log2 FC of 1 and -1 (horizontal) and mean normalized count = 100 (vertical). Up- and down-regulated genes are colored orange or blue, respectively. **(B)** Principal component analysis of DESeq normalized rlog counts with cell treatment information shown by color. LeGO-Ctl (n = 2), and LeGO-473ox (n = 2) are shown in orange and blue, respectively. **(C)** Hierarchical clustering analysis of gene expression profiles across samples using DESeq normalized rlog counts. FLC cells with LINC00473

overexpression (LeGO-473ox) or empty vector control (LeGO-Ctl) are indicted by orange and blue boxes, respectively. **(D)** Normalized counts for specific FLC marker genes from RNA-seq from LeGO-473ox and LeGO-Ctl control FLC monoclonal cells. **(E, F)** MSigDB Hallmark or KEGG pathway enrichment analysis of 1403 genes in (A) and 1374 genes in (B), respectively. Pathways with p-value < 0.05 represented in figure. Color represents the -log10 p-value. Normalized counts for metabolism-related genes from RNA-seq from LeGO-473ox and LeGO-Ctl control FLC monoclonal cells. **(G)** EdU incorporation in FLC cells with stable LINC00473 knockdown (sh473) compared to control (shCtl), and LINC00473 overexpression (LeGO-473ox) compared to control (LeGO-Ctl). Representative images of DAPI- and EdU-stained cells show total and proliferative cells, respectively. **(H)** TUNEL staining in FLC cells with stable LINC00473 knockdown (sh473) compared to control (shCtl), and LINC00473 overexpression (LeGO-473ox) compared to control (LeGO-Ctl). Representative images of DAPI- and TUNEL-stained cells show total and apoptotic cells, respectively. **(I)** Gene list overlap analysis using significantly up-regulated genes in FLC tumors relative to NML (n = 1667), and in LeGO-473ox cells relative to control (n = 1403). Bolded genes indicate proteins related to metabolism. Elsevier pathway enrichment analysis of the intersecting 188 genes. Color indicates the -log10 adjusted p-value, and significance of the overlap ($p=4.81x10^{-20}$) was calculated by hypergeometric test. **(J)** Gene list overlap analysis using significantly down-regulated genes in FLC tumors relative to NML (n = 1497), and in LeGO-473ox cells relative to control (n = 1374). Bolded genes indicate proteins related to apoptosis. MSigDB Hallmark pathway enrichment analysis of the intersecting 91 genes. Color indicates the -log10 adjusted p-value. Overlap of n = 91 genes was not significant following a hypergeometric test. Bar chart data in G and H are represented as mean across n = 6 ± SD. Scale bars represent 100 μm. P values are calculated by 2-tailed Student's t-test. *p < 0.05, **p < 0.01, ***p < 0.001 unless otherwise indicated.

Figure 5. LINC00473 increases glycolysis and alters mitochondrial activity in FLC. (A) Representative graph of extracellular acidification rate (ECAR) of FLC cells with stable LINC00473 overexpression (LeGO-473ox) and empty vector control (LeGO-Ctl). **(B)** Quantification of glycolysis, glycolytic capacity and glycolytic reserve in LINC00473-overexpression (LeGO-473ox) FLC cells compared to empty-vector control (LeGO-Ctl). **(C)** Representative graph of ECAR of FLC cells with stable LINC00473 knockdown (sh473) and non-targeting control (shCtl). **(D)** Quantification of glycolysis, glycolytic capacity and glycolytic reserve in LINC00473-knockdown (sh473) FLC cells compared to non-targeting control (shCtl). Data are representative of 2 or 3 independent trials, respectively, of n = 5 replicates per experiment. **(E)** Representative graph of oxygen consumption rate (OCR) of FLC cells with overexpression (LeGO-473ox) and control (LeGO-Ctl). **(F)** Quantification of basal respiration, maximum respiration capacity, and spare respiratory capacity in LINC00473-overexpression (LeGO-473ox) FLC cells compared to empty-vector control (LeGO-Ctl). **(G)** Representative graph of OCR of FLC cells with stable LINC00473 knockdown (sh473) and non-targeting control (shCtl). **(H)** Quantification of basal respiration, maximum respiration capacity, and spare respiratory capacity in LINC00473-knockdown (sh473) FLC cells compared to non-targeting control (LeGO-Ctl). Data are representative as mean ± SD across 2 or 3 independent trials, respectively, of n = 5 replicates per experiment. P values are calculated by 2-tailed Student's t-test. *p < 0.05, **p < 0.01, ***p < 0.001.

Figure 6. LINC00473 is a regulator of FLC tumor growth in vivo. (A) Growth curves of subcutaneous tumors following transplantation of FLC monoclonal cells into the flank of NOD–Scid–Il2rg-deficient (NSG) mice. Tumors formed from transplantation of FLC monoclonal cells with stable LINC00473 overexpression (LeGO-473ox) and empty vector control (LeGO-Ctl). Relative tumor volume is determined as the percent growth compared to initial volume at Day 0 when tumors were first detectable and measured with calipers. n = 8 per group (4 female, 4 male). Data are represented as mean ± SD. **(B)** Individual growth curves of each subcutaneous tumor in (A). n = 4 mice per trial; 2 independent trials were conducted. **(C)** Gene expression of DP fusion transcript and LINC00473 from RT-qPCR in LINC00473-overexpression (LeGO-473ox) and empty-vector control (LeGO-Ctl) subcutaneous FLC tumors. Statistical testing on tumor growth was performed using a 2-tailed Student's t-test following area under the curve analysis using the definite integral of each fitted polynomial function. Otherwise, P values are calculated by 2-tailed Student's t-test. *p < 0.05, **p < 0.01, ***p < 0.001.

Figure 7. Model of LINC00473 function in FLC. Summary of the upstream regulators of LINC00473 and its role in regulating FLC-marker gene expression, glycolysis and mitochondrial energetics, and cancer cell expansion *in vitro* and *in vivo* to promote tumor growth in fibrolamellar carcinoma. Black arrows are directly supported by our study; grey arrows and proteins were previously reported in other cancer types.

Methods

Primary tumor samples and PDX tumors

FLC tumors and NML

Cohort 1. Informed consent was obtained from all human subjects. FLC and non-malignant liver samples were collected from FLC patients according to Institutional Review Board protocols 1811008421 (Cornell University) or 33970/1 (Fibrolamellar Cancer Foundation) and provided by the Fibrolamellar Cancer Foundation. All samples were de-identified prior to shipment to Cornell University and were collected from both male and female subjects and importantly, some samples were collected from the same patient

Cohort 2. Informed consent was obtained from all human subjects. FLC and non-malignant liver samples were collected from female and male FLC patients according to Institutional Review Board protocol 1765.

PDX tumors

Mice. Animal care, facilities, procedures, and technical services used in this study are in compliance with NIH regulations, the Cornell University Institutional Animal Care and Use Committee (protocol 2017-0035), and the Association for the Assessment and Accreditation of Laboratory Animal Care (AAALAC) International. All animal research space and supporting equipment are controlled by technicians, residents, and board-certified laboratory animal veterinarians of the Center for Animal Resources and Education (CARE).

Mouse strains and husbandry. NOD.Cg-*Prkdc*^{scid} *Il2rg*^{tm1Wjl}/SzJ (NSG) mice catalog number 005557 were sourced from The Jackson Laboratory and bred at Cornell with the supervision of the Center for Animal Resources and Education (CARE) breeding program.

PDX tumor maintenance and passaging. At the time of passaging, tumors (diameter of 0.5cm) are transplanted subcutaneously into the flank of NSG mice (male and female, 6-10 weeks of age). Each mouse harbors a single tumor. Animals are housed in ventilated cages with *ad libitum* access to food and water. Mice are monitored for signs of distress, such as poor grooming and weight loss until the endpoint, which is established when PDX tumors reach a diameter of 3cm at any greatest dimension. Mice are subsequently euthanized for tumor collection, which is divided for propagating tumor passaging. Procedures are performed according to protocols approved by the Cornell University Institutional Animal Care and Use Committee.

RNA-seq, snATAC-seq and ChRO-seq

RNA isolation: For RNA purification from tissues, 15-30mg of flash-frozen patient samples and patient-derived xenograft tumors were pulverized using dry-ice chilled Bessman Tissue Pulverizer Thomas Scientific, 1210V37). Each sample was hammered 4 times with a one-quarter turn of the hammer until tissues became a fine powder and transferred to 1.5mL Eppendorf tubes containing 600uL lysis buffer (Total RNA Purification Kit, Norgen Biotek, 17200). Incubated on ice for 30 minutes prior to homogenization using Polytron System PT 1200E for 30s. Samples were centrifuged at 14,000RPM for 2 minutes and the supernatant was collected as tissue homogenate in a clean 1.5mL tube for immediate RNA purification. The tissue pulverizer was cleaned with 70% ethanol and RNase Away, and chilled in dry ice for 2 minutes between sample preparations. The polytron was cleaned in three washes of water and RNase Away between sample processing. RNA was extracted from tissue homogenates and cells using the Total RNA Purification Kit (Norgen Biotek, 17200) according to the manufacturer's instructions. RNA concentrations were measured using Nanodrop One and RNA integrity was quantified using the 4200 Tapestation.

RNA-seq. Gene expression was analyzed in 35 FLC and 10 non-malignant liver (NML) samples. Of these, 16 FLC and 2 NML samples were published previously (accession: EGAS00001004169)[52].The remaining 19 FLC and 8 NML samples represent a cohort of samples with new RNA-seq data provided by this study (accession: TBD) and were previously published with small RNA-seq data (accession: GSE181922). As with the published samples, RNA was isolated from the new cohort using the Total RNA Purification Kit (Norgen Biotek). Libraries were prepared using the

NEBNext Ultra II Directional Library Prep Kit following PolyA enrichment at the Cornell Transcriptional Regulation and Expression Facility (Cornell University, Ithaca, NY). Libraries were then sequenced using the NextSeq500 platform (Illumina).

Sequencing results were aligned to the human genome (hg38) using STAR (v2.4.2a) and quantified using Salmon (v0.8). Differential expression of genes was determined using DESeq2 (v1.29). Genes with an average expression of less than 5 (base mean) were discarded from the analysis. Enrichr was used for pathway analyses as described in Chen et al[61]. Our RNA-seq datasets on patient tissues, as well as LeGO-473ox and LeGO-Ctl cells, were deposited into the Gene Expression Omnibus (GEO: GSE233148).

snATAC-seq: Single-nucleus ATAC (snATAC) analysis was performed as previously described[59]. Data generated from our snATAC-seq studies were previously published and are available at the Gene Expression Omnibus through accession number GSE202315.

ChRO-seq: Chromatin Run-On sequencing (ChRO-seq) analysis was performed as previously described[52]. Data can be downloaded from the European Genome-Phenome Archive through the European Genome-Phenome Archive via accession number EGAS00001004169.

RT-qPCR

RNA was extracted from tissue homogenates and cells using the Total RNA Purification Kit (Norgen Biotek, 17200) according to the manufacturer's instructions. RNA concentrations were measured using Nanodrop One and 0.25ug of RNA for gene analysis was used for reverse transcription using the High-Capacity RNA-to-cDNA Kit (Applied Biosystems, 4368814) according to manufacturer instructions. Quantification of gene expression was done using the TaqMan Gene Expression Master Mix (ThermoFisher Scientific, Waltham, MA). Gene expression was normalized to RPS9 (assay ID: Hs02339424_g1). qPCR was performed using the BioRad CFX96 Touch Real-Time PCR Detection System (Bio-Rad Laboratories, Richmond, CA).

Gene Taqman assays:

DNAJB1-PRKACA (assay ID: AIHSPSH)
PRKACA (custom assay ID: AIS093C)
DNAJB1 (assay ID: Hs00428680_m1)
LINC00473 TV1 (custom assay ID: APT2A4G)
LINC00473 TV2 (custom assay ID: APRWGJJ)
U6 (assay ID: 001,973)
tRNA-Glycine (custom assay ID: CS1RUHV)
CTNNB1 (assay ID: Hs00355045_m1)
SLC16A14 (assay ID: Hs005431300_m1)
VCAN (assay ID: Hs0017642_m1)
RPS9 (assay ID: Hs02339424_g1)

Subcellular Fractionation

FLC cells were washed and pelleted in PBS at 1 x 10^6 for subcellular fractionation as previously described[82]. Briefly, cell pellets were lysed in RLN1 buffer (50 mM Tris-HCl pH 8.0, 140 mM NaCl, 1.5 mM MgCl2, 0.5% NP-40, 40 units/mL RNAse inhibitor) on ice for 5 min and subsequently centrifuged at 500g for 2 min. The cytoplasm contained in the supernatant was isolated from the pelleted nuclear fraction. RNA was isolated from both fractions using Total RNA Purification Kit (Norgen Biotek, 17200) as per manufacturer instructions. RNA concentration was quantified using Nanodrop One. Equal amounts of RNA and cDNA were used for subsequent reverse transcriptase reactions and qPCR, as described above. All samples were tested for U6 (nuclear control) and tRNA-Glycine (cytoplasmic control). The sum of nuclear and cytoplasmic RNA expression levels of each gene was set to 100% and the percentage of each transcript localized to each compartment was calculated. For U6 and tRNA-Glycine, reverse transcription was performed using 0.2ug of RNA and TaqMan MicroRNA Reverse Transcription Kit (ThermoFisher, 4311235), followed by qPCR using TaqMan Universal PCR Master Mix (ThermoFisher, 4324018). Data represents 3 biological replicates.

Cell lines

FLC cells. FLC cells were previously described by Francisco et al., generated from a patient-derived xenograft model developed by Oikawa et al. and were a generous gift from Dr. Nabeel Bardeesy[60,83]. FLC cells were grown in complete RPMI media (RPMI 1640, Gibco 11875119; 10% FBS, heat-treated at 56˚C for 30 minutes, Gibco 26140079; 1% penicillin-streptomycin, Gibco 15140122; and 25ng/mL human hepatic growth factor, Gibco PHG0321).

LINC00473 Overexpression and Knockdown cell lines: To enable LINC00473 knockdown via lentiviral integration of shRNA, our collaborators in the Wu Lab at the University of Florida generously gifted us lentiviral vector harboring short hairpin RNAs (shRNAs) targeting LINC00473 (sh473-2, sh473-4) and control (shCtl) that were previously used to downregulate gene expression in human lung cancer cell lines[47]. The pLKO.1 cloning vector served as the plasmid backbone, which is a replication-incompetent lentiviral vector encoding a puromycin resistance marker[84]. Two independent shRNA oligos targeting LINC00473 were individually cloned into pLKO.1 at the EcoRI and AgeI restriction sites, and subsequently transformed and replicated in DH5-Alpha E. coli cells under ampicillin selection. Next, the oligo insert was screened following restriction digest with EcoRI and NcoI for gel electrophoresis and sanger sequencing using the pLKO.1 sequencing primer. Next, lentiviral particles were produced by transfecting the pLKO.1 shRNA plasmid combined with the psPAX2 packaging plasmid and the pMD2.G envelope plasmid into HEK293T cells. Over 4 days, virus-containing media was harvested for virus isolation using Lenti-X concentrator, Takara) in lieu of ultracentrifugation. After performing puromycin kill curve assays in FLC and HEK293-DP cells, lentiviral particles were titered in a range of dilutions in DMEM complete (DMEM with 10% FBS and 2% Glutamax) and 10ug/mL polybrene and subsequently introduced to target cells using reverse transduction in order to generate a Poisson distribution curve of a viral multiplicity of infection (MOI). An MOI of 0.3 was selected for viral transduction to achieve a predicted single viral integration in 22% of treated cells while reducing the cell population with >1 integration to only 4%. Following puromycin selection, the majority of transduced FLC cells will express a single copy of shRNA to mitigate off-target effects, enabling the selection of a stable polyclonal cell culture. Polyclonal cells were grown across 5 passages and verified for stable gene knockdown using RT-qPCR. Conditioned medium was collected during cell growth. Next, monoclonal cell populations were generated by limiting dilution by seeding an average of 0.5 cells per well in 96-well plates in presence of conditioned medium and puromycin. This ensures that some wells receive a single cell while minimizing the chance that any well is seeded with >1 cell. Cells were grown undisturbed for 14 days, and wells with expanded cell populations were transferred to larger culture dishes. Each monoclone was subsequently expanded and gene knockdown was validated via RT-qPCR. Monoclonal cell lines with robust LINC00473 downregulation were selected for functional assessments in vitro and in vivo.

To develop stable LINC00473 overexpression via lentiviral integration of cDNA, the LeGO-lnc cloning vector served as the plasmid backbone (a gift from Dr. Jan-Henning Klusmann, Addgene plasmid #80624), which is a replication-incompetent lentiviral vector encoding a blasticidin resistance marker. A double-stranded cDNA clone of LINC00473 was designed based on the human sequence from the UCSC genome browser, and subsequently synthesized and purchased from Integrated DNA Technologies (gBlocks Gene Fragment). The cDNA was cloned into LeGO-lnc at the NotI and SFFV restriction sites, and subsequently transformed and replicated in DH5-Alpha E. coli cells under ampicillin selection. Next, the cDNA oligo insert was screened following restriction digest with NotI and PacI for gel electrophoresis and Sanger sequencing using the SFFV forward primer and MSCV reverse primer. Next, lentiviral particles were produced by transfecting the LeGO-LINC00473 plasmid combined with the psPAX2 packaging plasmid and the pMD2.G envelope plasmid into HEK293T cells. Over 4 days, virus-containing media was harvested for virus isolation using Lenti-X concentrator (Takara) in lieu of ultracentrifugation. The methods performed for generating polyclonal and monoclonal cell lines harboring LINC00473 overexpression and control are described above; however, antibiotic selection was enabled using blasticidin.

HepG2-DP and HepG2-Ctl: HepG2-DP cells were previously described and were a generous gift from Dr. Sean Ronnekleiv Kelly[76]. Briefly, the *DNAJB1-PRKACA* expressing HepG2 cells (HepG2-DP) were generated using a mammalian dual-guide RNA-CRISPR-CAS9-EGFP vector (VectorBuilder,

Chicago, IL) with guide RNA sequences targeting the first intronic regions of *DNAJB1* and *PRKACA* (gRNA1 (DNAJB1) 5'-CAGGAGCCGACCCCGTTCGT-3', gRNA2 (PRKACA): 5'-GTAGACGCGGTTGCGCTAAG-3'). Genomic DNA and mRNA were used to confirm the presence of *DNAJB1-PRKACA* fusion as previously described[76]. Cells were grown in DMEM complete media (DMEM, high glucose, Gibco, 11965092; 10% FBS, heat-treated at 56C for 30 minutes, Gibco, 26140079; 5% penicillin-streptomycin 10,000U/mL, Gibco, 15140122; 5% Glutamax 100X, Gibco, 35050061).

HEK293-DP and HEK293-WT: HEK293-DP cells expressing DNAJB1-PRKACA have been previously described and were a generous gift from Dr. Khashayar Vikili[51]. Cells were grown in DMEM complete media (DMEM, high glucose, Gibco, 11965092; 10% FBS, heat-treated at 56C for 30 minutes, Gibco, 26140079; 5% penicillin-streptomycin 10,000U/mL, Gibco, 15140122; 5% Glutamax 100X, Gibco, 35050061; 5% sodium pyruvate 100mM, Gibco, 11360070).

In vitro assays on cell growth, colony growth, viability, and apoptosis

Cell growth curve. Lentiviral-transduced FLC cells were seeded in a 24-well plate at a density of 50,000 cells per well (Day 0). Daily counts were performed for 6 days in approximate 24-hour intervals after initial seeding. Cells were washed in PBS (calcium and magnesium-free; Gibco, 10010023) and coated with 200uL 0.25% trypsin-EDTA (Gibco, 25200056) followed by 5 min incubation at 37°C or until 90% of cells detached from the well. Various volumes of pre-warmed complete RPMI media (RPMI 1640, Gibco 11875119; 10% FBS, heat-treated at 56°C for 30 minutes, Gibco, 26140079; 1% penicillin-streptomycin, Gibco 15140122) were used to resuspend cells, specifically, 200uL on Day 1; 300uL on Day 2; 800uL on Day 3, 1600uL on Day 4, and 2000uL on Days 5-6. 10uL of cell suspension was transferred to a hemocytometer (Bright-Line, Z359629) and observed under a microscope under a 10X objective lens. Cells were counted from the large, central gridded square ($1mm^2$) and multiplied by 10^4 to calculate the number of cells per mL, and subsequently multiplied by the total volume of the cell resuspension (mixture of 0.5% trypsin-EDTA and complete media; ranges from 400uL to 2200uL) to determine the total number of cells per well. Cells were prepared for counting in groups of 4 wells to avoid over-trypsinization and clumping. The protocol for evaluating cell growth in transduced HEK293-DP cells was performed as previously reported by Kim et al.[51].

Soft agar assay. 6-well plates were coated with 0.6% UltraPure Low Melting Point Agarose (Invitrogen, 16520050) mixed with complete RPMI media (RPMI 1640, Gibco 11875119; 10% FBS, heat-treated at 56C for 30 minutes, Gibco, 26140079; 1% penicillin-streptomycin, Gibco 15140122). Transduced FLC cells were suspended in 0.3% agarose and seeded in 6-well plates at a density of 10,000 cells per well. Once solidified, an additional layer of 0.3% agarose was added to coat each well. Plates were incubated at 37C for a colony growth period of 8 days. Cells were fixed and stained with 200uL of 1 mg/mL solution of Nitro Blue Tetrazolium Chloride (Invitrogen, N6495). Six biological replicates were performed, and 10-12 independent fields of view were imaged per well. Colony area was quantified using FIJI software. Data represents the cell colony growth as a percent of the total area per image.

EdU-incorporation assay. 72 hours after seeding in 96-well plates at a density of 3500 cells per well, cells were incubated with 10 μM EdU at 37 °C in complete media for 2 h. Cells were then fixed with 4% paraformaldehyde for 20 min at room temperature and permeabilized using 0.5% Triton X-100 in PBS for 20 min. The Invitrogen Click-iT Plus EdU AlexaFluor 488 Imaging Kit (Invitrogen, Waltham, MA, C10637) was used to detect EdU according to the manufacturer's instructions. Nuclei were stained using DAPI (ThermoFisher, D1306) and imaged using ZOE Fluorescent Cell Image (Bio-Rad Laboratories, Richmond, CA). Images were analyzed using FIJI. For EdU-positive cells, the threshold value was set to 10. For analyzing particles, counted those particles with size = 250-Infinity and circularity = 0.4–1.

TUNEL assay. 72 hours after seeding in a 96-well plate at a density of 3500 cells per well, cells were washed twice with PBS and fixed using 4% paraformaldehyde for 15 min at room temperature. Permeabilization was performed by using 0.5% Triton X-100 in PBS for 20 min. Cells were washed twice with deionized water. Positive control wells were treated with 1X DNase I, Amplification Grade (ThermoFisher, 18,068–015) solution according to the manufacturer's instructions. Labeling and

detection of apoptotic cells were completed using the Invitrogen Click-iT Plus TUNEL Assay for In Situ Apoptosis Detection 488 kit (Invitrogen, Waltham, MA, catalog #: C10617) according to the manufacturer's instructions. Nuclei were stained using DAPI (ThermoFisher, D1306) and imaged using ZOE Fluorescent Cell Image (Bio-Rad Laboratories, Richmond, CA). Images were analyzed using FIJI. For TUNEL-positive cells, the threshold value was set to 14. For analyzing particles, counted those particles with size = 250-Infinity and circularity = 0.4–1.

Subcutaneous cell transplantation and tumor growth

FLC monoclonal cell lines overexpressing LINC00473 (LeGO-473ox) or empty vector control (LeGO-Ctl) were established as described above. Expression of key genes of interest, including *DNAJB1-PRKACA*, *LINC00473*, and *RPS9* control, was assessed via RT-qPCR (as previously described) across 5 independent passages per monoclone to validate stable gene expression. Two weeks prior to transplantation, cells were grown in absence of antibiotics and submitted for mycoplasma testing. Cells were washed and resuspended in ice-cold PBS and mixed with an equal volume of matrigel for single-flank injections of 2 million cells in 200uL per animal. Mice were monitored twice a week to monitor for palpable tumors, and after initial tumor detection (denoted as Day 0), tumor volumes were quantified three times a week using digital calipers. Mice were euthanized and tumors were collected 7 days after initial tumor detection. Relative tumor % growth is calculated as (tumor volume at Day N/ the tumor volume at Day 0) x 100%.

Western Blot

FLC cells were lysed in RIPA buffer containing Halt Protease and Phosphatase Inhibitor Cocktail (ThermoFisher, 78441) at 4°C. Cells were incubated for 30 minutes and centrifuged at 14,000g for 10 minutes at 4°C. Total protein in the supernatant was quantified using the Pierce BCA Protein Assay Kit (ThermoFisher, 23225). Samples were denatured in NuPAGE LDS Sample Buffer (ThermoFisher NP0007) containing 5% β-Mercaptoethanol for 10 minutes at 70°C and loaded to a 10% NuPAGE gel (ThermoFisher, NP0301BOX). After electrophoresis, samples were transferred to polyvinylidene difluoride membranes and blocked in 3% bovine serum albumin (BSA) in tris-buffered saline and 0.5% Tween 20 (TBST) for 1 hour at room temperature. Membranes were incubated in primary antibodies at 4C overnight. Membranes were subsequently incubated in secondary antibodies at room temperature for 1 hour followed by three washes of TBST. Immunoblots were visualized using an enhanced chemiluminescence (ECL) kit (Cytiva, 89238-012) and a ChemiDoc MP (Bio-Rad).

The antibodies used in this study consisted of PRKACA (1:1000 dilution, Cell Signaling Technology, 4782), HSP40 (1:1000 dilution, Santa Cruz Biotechnology, sc-398766), Vinculin (1:1000 dilution, Santa Cruz Biotechnology, sc-73614), mouse IgG secondary antibody (1:2000, Santa Cruz Biotechnology, sc-525409), and rabbit IgG secondary antibody (1:2000, Cell Signaling Technology, 7074). Protein quantification was performed using FIJI software (normalized to vinculin; loading controls were run on the same blot).

siRNAs

siRNA synthesis and LNP formulation. All oligonucleotides were prepared using commercially available 5′-O-DMT-3′-O-(2-cyanoethyl-N,N-diisopropyl) phosphoramidite monomers by following standard protocols for solid phase synthesis and deprotection[85,86]. The PS linkages were introduced by the oxidation of phosphite utilizing 0.1 M N,N-dimethyl-N'-(3-thioxo-3H-1,2,4-dithiazol-5-yl)methanimidamide (DDTT) in pyridine. The *N*-acetylgalactosamine (GalNAc) ligand was introduced to the 3′-end of the sense strand of the siRNA using a functionalized solid support as described[87]. 2'-O-hexadecyl (C16) and cholesterol (chol)-functionalities were introduced as described elsewhere[88,89]. After deprotection, single strands were purified by ion-exchange HPLC followed by desalting and annealing of equimolar amounts of complementary strands to provide the desired siRNAs and siRNA conjugates. Lipid nanoparticles (LNPs) containing encapsulated siRNAs were formulated as described previously[90].

siRNA in vitro activity by transfection. siRNA efficacy for gene silencing was initially evaluated by reverse transfection on FLC cells in 48-well plates. 20 uL solutions of siRNA were prepared at 10X

concentration in PBS and subsequently mixed with OptiMEM (Gibco 31985062) and Lipofectamine RNAiMax Transfection Reagent (Invitrogen 13778030) according to manufacturer instructions. After 30 min incubation at room temperature, the mixture was transferred to wells. Next, FLC cells were plated at a density of 34000 cells per well for a final volume of 200 uL. The final concentration of siRNAs was 50 nM. Plates were gently rocked by hand from side to side after plating and incubated at 37C for 48 hours prior to cell preparation for RNA isolation.

Transfection of siPKA and non-targeting controls in FLC cells was performed using siGENOME single and SMARTpool siRNA PRKACA from Dharmacon. For siRNA treatment, 12 µl of 20 µM siRNA was added to the cells with Lipofectamine RNAiMAX reagent in Opti-MEM, incubated for 72 hr, and harvested for subsequent RNA isolation.

Free-Uptake. To test the efficacy of different siRNA delivery strategies in FLC cells, we performed free uptake studies in FLC cells with CTNNB1-targeting siRNAs that were conjugated to N-acetylgalactosamine (GalNAc), 2′-O-hexadecyl (C16), cholesterol (chol), or encapsulated LNPs. 20 uL solutions of siRNA were prepared at 10X concentration and transferred to wells. FLC cells were plated at a density of 34000 cells per well for a final volume of 200 uL. Plates were gently rocked by hand from side to side after plating and incubated at 37C for 48 hours. The final concentrations of GalNAc-, C16, and chol-conjugated siRNAs were 50 nM and 500 nM. The final concentrations of LNP-siRNAs were 2.5nM, 12.5 nM, 62.5 nM, and 312.5 nM.

To test gene silencing of the DP fusion using siDP#1-LNP and siDP#2-LNP, free-uptake was performed on FLC cells as described above using 6-well plates for a final volume of 2mL and final siRNA concentration of 5nM at 37C for 96 hours. At the end of incubation, a portion of the cell suspension was allocated for RNA purification and the remainder was used for protein isolation. Data shown represent at least 3 biological replicates.

Seahorse assay

Extracellular acidification rate (ECAR) measures pH changes as cells produce lactate, and thus serves as a proxy for glycolysis. Cells were plated on XFe24 cell culture plates at the following seeding densities: A3 – 91,000 cells per well; C2 – 60,000 cells per well; D3 – 57,000 cells per well; F6 – 81,000 cells per well, and incubated for 48-hour at 37°C with 5% CO_2. Following incubation, cells were washed in PBS and culture media was replaced with unbuffered Dulbecco's Modified Eagle's Medium (DMEM) supplemented with 2 mM L-glutamine. The compound concentrations for the mitochondrial stress test were as follows (final concentration): Port A: Glucose (11 mM), Port B: Oligomycin (1 µM), and Port C: 2-Deoxy-D glucose (50 mM). The ECAR was normalized to the total cell number using the Celigo image cytometer. Respirometry data were collected using Agilent Wave v2.4 software and were expressed as mean ± SEM. To evaluate glucose metabolism, ECAR is measured in response to the addition of D-glucose in order to activate glycolysis, oligomycin to shut down oxidative phosphorylation and subsequently stimulate maximal glycolytic capacity, and deoxy-D-glucose (2-DG), a competitive inhibitor of glucose that blocks glycolysis. Glycolytic reserve capacity was calculated by subtracting glycolysis from maximum glycolytic capacity.

Oxygen consumption rate (OCR) was measured by the Agilent Seahorse XFe 24 Bioanalyzer. Cells were plated on XFe24 cell culture plates at the following seeding densities: A3 – 91,000 cells per well; C2 – 60,000 cells per well; D3 – 57,000 cells per well; F6 – 81,000 cells per well, and incubated for 48-hour at 37°C with 5% CO_2. Following incubation, cells were washed in PBS and culture media was replaced with unbuffered Dulbecco's Modified Eagle's Medium (DMEM) supplemented with 4.5 g/L glucose, 4 mM glutamine, and 1 mM pyruvate. The compound concentrations for the mitochondrial stress test were as follows (final concentration): Port A: Oligomycin (1 µM), Port B: Carbonyl cyanide-4 (trifluoromethoxy) phenylhydrazone (FCCP) (1 µM), Port C: Rotenone/Antimycin A (2 µM) each. The OCR was normalized to the total cell number using the Celigo image cytometer. Respirometry data were collected using Agilent Wave v2.4 software and were expressed as mean ± SEM. To evaluate mitochondrial respiration, OCR is measured in response to a series of modulators that alter electron transport chain function. Specifically, treatment with oligomycin inhibits ATP synthase and subsequently blocks respiration. Next, carbonyl cyanide 4-trifluoromethoxyphenylhydrazone (FCCP) acts as an uncoupling agent that stimulates the ETC to operate at maximum capacity, revealing maximum

respiratory capacity. Lastly, antimycin A and rotenone (R/A), inhibitors of complex III and I, are added to shut down ETC function, uncovering non-mitochondrial respiration. Spare Respiratory Capacity (SRP) is calculated by subtracting basal respiration from maximum respiratory capacity.

Acknowledgements

We are grateful for the support provided by Rishi Puri and Scott Butler at the PATh PDX Facility and the Cornell Transcriptional Regulation and Expression Facility at Cornell University (Cornell University, Ithaca, NY). We thank past and current members of the Sethupathy lab for helpful discussions and support, and Jonathan Villanueva for assistance in computational analysis of ChRO-seq. We thank the Alnylam bioinformatics, high-throughput synthesis and RNAi lead discovery team for designing, synthesizing and screening the siRNAs. We are grateful to the FLC patient donors whose contributions make this work possible. Figure schematics were created with BioRender.com.

This work was supported by funding from the College of Veterinary Medicine Scholarship (awarded to RKM), Center for Vertebrate Genomics Scholar Award (awarded to RKM), Sandra Atlas Bass Endowment for Cancer Research (awarded to PS), and the Fibrolamellar Cancer Foundation (awarded to PS).

Contributions

Conception and design: R.K. Ma and P. Sethupathy
Acquisition of data: R.K. Ma, P-Y. Tsai
Analysis and interpretation of data: R.K. Ma, A.R. Farghli, P-Y. Tsai, A. Shumway, M. Kanke, J.D. Gordan, T.S. Gujral, K. Vakili, M. Nukaya, L. Noetzli, S. Ronnekleiv-Kelly, W. Broom, J. Barrow, P. Sethupathy
Writing -- original draft: R.K. Ma, P. Sethupathy
Writing – review and editing: All authors, especially R.K. Ma, M. Kanke, T.S. Gujral, S. Ronnekleiv-Kelly, P. Sethupathy
Study supervision: P. Sethupathy

Declaration of Interests

Drs. Wendy Broom and Leila Noetzli are employees and shareholders of Alnylam Pharmaceuticals, with multiple patent applications pending. All other authors declare no competing interests.

References

1. Mavros, M. N., Mayo, S. C., Hyder, O. & Pawlik, T. M. A Systematic Review: Treatment and Prognosis of Patients with Fibrolamellar Hepatocellular Carcinoma. *J. Am. Coll. Surg.* **215**, 820–830 (2012).
2. Graham, R. P. & Torbenson, M. S. Fibrolamellar carcinoma: A histologically unique tumor with unique molecular findings. *Semin. Diagn. Pathol.* **34**, 146–152 (2017).
3. El-Serag, H. B. & Davila, J. A. Is Fibrolamellar Carcinoma Different from Hepatocellular Carcinoma? A US Population-Based Study. *Hepatology* **39**, 798–803 (2004).
4. Dinh, T. A. *et al.* A framework for fibrolamellar carcinoma research and clinical trials. *Nat. Rev. Gastroenterol. Hepatol.* **19**, 328–342 (2022).
5. O'Neill, A. F. *et al.* Fibrolamellar carcinoma: An entity all its own. *Curr. Probl. Cancer* **45**, 100770 (2021).
6. Lalazar, G. & Simon, S. M. Fibrolamellar Carcinoma: Recent Advances and Unresolved Questions on the Molecular Mechanisms. *Semin. Liver Dis.* **38**, 51–59 (2018).
7. Riggle, K. M., Turnham, R. E., Scott, J. D., Yeung, R. S. & Riehle, K. J. Fibrolamellar Hepatocellular Carcinoma: Mechanistic Distinction From Adult Hepatocellular Carcinoma. *Pediatr. Blood Cancer* **63**, 1133–1316 (2016).
8. Mayo, S. C. *et al.* Treatment and Prognosis of Patients with Fibrolamellar Hepatocellular Carcinoma: A National Perspective. *J. Am. Coll. Surg.* **218**, 196–205 (2014).
9. Ang, C. S. *et al.* Clinicopathologic characteristics and survival outcomes of patients with Fibrolamellar carcinoma: Data from the Fibrolamellar Carcinoma consortium. *Gastrointest. Cancer Res.* **6**, 3–9 (2013).
10. Stipa, F. *et al.* Outcome of patients with fibrolamellar hepatocellular carcinoma. *Cancer* **106**, 1331–1338 (2006).
11. Honeyman, J. N. *et al.* Detection of a Recurrent DNAJB1-PRKACA Chimeric Transcript in Fibrolamellar Hepatocellular Carcinoma. *Science (80-.).* **973**, 970–973 (2014).
12. Xu, L. *et al.* Genomic analysis of fibrolamellar hepatocellular carcinoma. *Hum. Mol. Genet.* **24**, 50–63 (2015).
13. Cornella, H. *et al.* Unique genomic profile of fibrolamellar hepatocellular carcinoma. *Gastroenterology* **148**, 806-818.e10 (2015).
14. Kastenhuber, E. R. *et al.* DNAJB1–PRKACA fusion kinase interacts with β-catenin and the liver regenerative response to drive fibrolamellar hepatocellular carcinoma. *Proc. Natl. Acad. Sci. U. S. A.* **114**, 13076–13084 (2017).
15. Engelholm, L. H. *et al.* CRISPR/Cas9 Engineering of Adult Mouse Liver Demonstrates That the Dnajb1–Prkaca Gene Fusion Is Sufficient to Induce Tumors Resembling Fibrolamellar Hepatocellular Carcinoma. *Gastroenterology* **153**, 1662-1673.e10 (2017).
16. Neumayer, C. *et al.* Oncogenic Addiction of Fibrolamellar Hepatocellular Carcinoma to the Fusion Kinase DNAJB1-PRKACA. *Clin. Cancer Res.* **29**, 271–278 (2023).
17. Schalm, S. S. *et al.* Evaluation of PRKACA as a Therapeutic Target for Fibrolamellar Carcinoma. *bioRxiv* 2022.01.31.477690 (2022). doi:10.1101/2022.01.31.477690
18. Averill, A. M. *et al.* Inhibition of the chimeric DnaJ-PKAc enzyme by endogenous inhibitor proteins. *J. Cell. Biochem.* **120**, 13783–13791 (2019).
19. Sullivan, K. M., Kenerson, H. L., Pillarisetty, V. G., Riehle, K. J. & Yeung, R. S. Precision oncology in liver cancer. *Ann. Transl. Med.* **6**, 285–285 (2018).
20. Sorenson, E. C. *et al.* Genome and transcriptome profiling of fibrolamellar hepatocellular carcinoma demonstrates p53 and IGF2BP1 dysregulation. *PLoS One* **12**, 1–17 (2017).
21. Dinh, T. A. *et al.* Comprehensive analysis of the Cancer Genome Atlas reveals a unique gene and non-coding RNA signature of fibrolamellar carcinoma. *Sci. Rep.* **7**, 1–15 (2017).
22. Simon, E. P. *et al.* Transcriptomic characterization of fibrolamellar hepatocellular carcinoma. *Proc. Natl. Acad. Sci. U. S. A.* **112**, E5916–E5925 (2015).
23. Hirsch, T. Z. *et al.* BAP1 mutations define a homogeneous subgroup of hepatocellular carcinoma with fibrolamellar-like features and activated PKA. *J. Hepatol.* **72**, 924–936 (2020).
24. Malouf, G. G. *et al.* Transcriptional profiling of pure fibrolamellar hepatocellular carcinoma reveals an endocrine signature. *Hepatology* **59**, 2228–2237 (2014).

25. Farber, B. A. *et al.* Non coding RNA analysis in fibrolamellar hepatocellular carcinoma. *Oncotarget* **9**, 10211–10227 (2018).
26. Dinh, T. A. *et al.* MicroRNA-375 Suppresses the Growth and Invasion of Fibrolamellar Carcinoma. *Cell Mol. Gastroenterol. Hepatol.* **7**, 803–817 (2019).
27. Turnham, R. E. *et al.* An acquired scaffolding function of the DNAJ-PKAc fusion contributes to oncogenic signaling in fibrolamellar carcinoma. *Elife* **8**, 1–27 (2019).
28. Chan, G. K. L. *et al.* Oncogenic PKA signaling increases c-MYC protein expression through multiple targetable mechanisms. *Elife* **12**, 1–28 (2023).
29. Quinodoz, S. & Guttman, M. Long noncoding RNAs: An emerging link between gene regulation and nuclear organization. *Trends Cell Biol.* **24**, 651–663 (2014).
30. Quinn, J. J. & Chang, H. Y. Unique features of long non-coding RNA biogenesis and function. *Nat. Rev. Genet.* **17**, (2016).
31. Uszczynska-Ratajczak, B., Lagarde, J., Frankish, A., Guigó, R. & Johnson, R. Towards a complete map of the human long non-coding RNA transcriptome. *Nat. Rev. Genet.* **19**, 535–548 (2018).
32. Kopp, F. & Mendell, J. T. Functional Classification and Experimental Dissection of Long Noncoding RNAs. *Cell* **172**, 393–407 (2018).
33. Wang, K. C. & Chang, H. Y. Molecular Mechanisms of Long Noncoding RNAs. *Mol. Cell* **43**, 904–914 (2011).
34. Mattick, J. S. The state of long non-coding RNA biology. *Non-coding RNA* **4**, (2018).
35. Ulitsky, I. & Bartel, D. P. LincRNAs: Genomics, evolution, and mechanisms. *Cell* **154**, 26 (2013).
36. Carlevaro-Fita, J. & Johnson, R. Global Positioning System: Understanding Long Noncoding RNAs through Subcellular Localization. *Mol. Cell* **73**, 869–883 (2019).
37. Schertzer, M. D. *et al.* lncRNA-Induced Spread of Polycomb Controlled by Genome Architecture, RNA Abundance, and CpG Island DNA. *Mol. Cell* **75**, 523-537.e10 (2019).
38. Ponting, C. P., Oliver, P. L. & Reik, W. Evolution and Functions of Long Noncoding RNAs. *Cell* **136**, 629–641 (2009).
39. Schmitt, A. M. & Chang, H. Y. Long Noncoding RNAs in Cancer Pathways. *Cancer Cell* **29**, 452–463 (2016).
40. Prensner, J. R. & Chinnaiyan, A. M. The emergence of lncRNAs in cancer biology. *Cancer Discov.* **1**, 391–407 (2011).
41. Balas, M. M. & Johnson, A. M. Exploring the mechanisms behind long noncoding RNAs and cancer. *Non-coding RNA Res.* **3**, 108–117 (2018).
42. Huarte, M. The emerging role of lncRNAs in cancer. *Nat. Med.* **21**, 1253–1261 (2015).
43. Arun, G., Diermeier, S. D. & Spector, D. L. Therapeutic Targeting of Long Non-Coding RNAs in Cancer. *Trends Mol. Med.* **24**, 257–277 (2018).
44. Li, J. *et al.* TANRIC: An interactive open platform to explore the function of lncRNAs in cancer. *Cancer Res.* **75**, 3728–3737 (2015).
45. Chiu, H. S. *et al.* Pan-Cancer Analysis of lncRNA Regulation Supports Their Targeting of Cancer Genes in Each Tumor Context. *Cell Rep.* **23**, 297-312.e12 (2018).
46. Redis, R. S. *et al.* Allele-Specific Reprogramming of Cancer Metabolism by the Long Non-coding RNA CCAT2. *Mol. Cell* **61**, 520–534 (2016).
47. Chen, Z. *et al.* cAMP/CREB-regulated LINC00473 marks LKB1- inactivated lung cancer and mediates tumor growth. *J. Clin. Invest.* **126**, 2267–2279 (2016).
48. Chen, Z. *et al.* CRTC1-MAML2 fusion-induced lncRNA LINC00473 expression maintains the growth and survival of human mucoepidermoid carcinoma cells. *Oncogene* **37**, 1885–1895 (2018).
49. Zhang, W. & Song, Y. LINC00473 predicts poor prognosis and regulates cell migration and invasion in gastric cancer. *Biomed. Pharmacother.* **107**, 1–6 (2018).
50. Zhang, L. *et al.* ZBTB7A Enhances Osteosarcoma Chemoresistance by Transcriptionally Repressing lncRNA LINC00473-IL24 Activity. *Neoplasia* **19**, 908–918 (2017).
51. Kim, S. S. *et al.* DNAJB1-PRKACA in HEK293T cells induces LINC00473 overexpression that depends on PKA signaling. *PLoS One* **17**, (2022).
52. Dinh, T. A. *et al.* Hotspots of Aberrant Enhancer Activity in Fibrolamellar Carcinoma Reveal

Candidate Oncogenic Pathways and Therapeutic Vulnerabilities. *Cell Rep.* **31**, 107509 (2020).
53. Liang, X. H. *et al.* Non-coding RNA LINC00473 mediates decidualization of human endometrial stromal cells in response to cAMP signaling. *Sci. Rep.* **6**, 1–9 (2016).
54. Pruunsild, P., Bengtson, C. P., Loss, I., Lohrer, B. & Bading, H. Expression of the primate-specific LINC00473 RNA in mouse neurons promotes excitability and CREB-regulated transcription. *J. Biol. Chem.* **299**, 104671 (2023).
55. Issler, O. *et al.* Sex-Specific Role for the Long Non-coding RNA LINC00473 in Depression. *Neuron* **106**, 912–926 (2020).
56. Pruunsild, P., Bengtson, C. P. & Bading, H. Networks of Cultured iPSC-Derived Neurons Reveal the Human Synaptic Activity-Regulated Adaptive Gene Program. *Cell Rep.* **18**, 122–135 (2017).
57. Tran, K. Van *et al.* Human thermogenic adipocyte regulation by the long noncoding RNA LINC00473. *Nat. Metab.* **2**, 397–412 (2020).
58. Chu, T. *et al.* Chromatin run-on and sequencing maps the transcriptional regulatory landscape of glioblastoma multiforme. *Nat. Genet.* **50**, 1553–1564 (2018).
59. Francisco, A. B. *et al.* Chemical, Molecular, and Single-nucleus Analysis Reveal Chondroitin Sulfate Proteoglycan Aberrancy in Fibrolamellar Carcinoma. *Cancer Res. Commun.* **2**, 663–678 (2022).
60. Francisco, A. B. *et al.* Multiomic analysis of microRNA-mediated regulation reveals a proliferative axis involving miR-10b in fibrolamellar carcinoma. *JCI Insight* **7**, (2022).
61. Chen, E. Y. *et al.* Enrichr: interactive and collaborative HTML5 gene list enrichment analysis tool. *BMC Bioinformatics* **14**, 128 (2013).
62. Lonsdale, J. *et al.* The Genotype-Tissue Expression (GTEx) project. *Nat. Genet.* **45**, 580–585 (2013).
63. Zhou, X. *et al.* Dependency of human and murine LKB1-inactivated lung cancer on aberrant CRTC-CREB activation. *Elife* **10**, 1–30 (2021).
64. Ruiz-Bañobre, J. *et al.* Noninvasive early detection of colorectal cancer by hypermethylation of the LINC00473 promoter in plasma cell-free DNA. *Clin. Epigenetics* **14**, 1–13 (2022).
65. Wein, M. N., Foretz, M., Fisher, D. E., Xavier, R. J. & Kronenberg, H. M. Salt-Inducible Kinases: Physiology, Regulation by cAMP, and Therapeutic Potential. *Trends Endocrinol. Metab.* **29**, 723–735 (2018).
66. Sun, Z., Jiang, Q., Li, J. & Guo, J. The potent roles of salt-inducible kinases (SIKs) in metabolic homeostasis and tumorigenesis. *Signal Transduct. Target. Ther.* **5**, (2020).
67. Patra, K. C. *et al.* Mutant GNAS drives pancreatic tumourigenesis by inducing PKA-mediated SIK suppression and reprogramming lipid metabolism. *Nat. Cell Biol.* **20**, 811–822 (2018).
68. Sakamoto, K., Bultot, L. & Göransson, O. The Salt-Inducible Kinases: Emerging Metabolic Regulators. *Trends Endocrinol. Metab.* **29**, 827–840 (2018).
69. Hollstein, P. E. *et al.* The AMPK-related kinases SIK1 and SIK3 mediate key tumor suppressive effects of LKB1 in NSCLC. *Cancer Discov.* **9**, 1606–1627 (2019).
70. Murray, C. W. *et al.* An Lkb1-Sik axis suppresses lung tumor growth and controls differentiation. *Cancer Discov.* **9**, 1590–1605 (2019).
71. Yang, R. *et al.* Role of INSL4 Signaling in Sustaining the Growth and Viability of LKB1-Inactivated Lung Cancer. *J. Natl. Cancer Inst.* **111**, 664–674 (2019).
72. Marchetti, P., Fovez, Q., Germain, N., Khamari, R. & Kluza, J. Mitochondrial spare respiratory capacity: Mechanisms, regulation, and significance in non-transformed and cancer cells. *FASEB J.* **34**, 13106–13124 (2020).
73. Burke, L. *et al.* The Janus-like role of proline metabolism in cancer. *Cell Death Discov.* **6**, (2020).
74. Schwörer, S. *et al.* Proline biosynthesis is a vent for TGFβ-induced mitochondrial redox stress. *EMBO J.* **39**, 1–20 (2020).
75. Armstrong, J. A. *et al.* Oxidative stress alters mitochondrial bioenergetics and modifies pancreatic cell death independently of cyclophilin D, resulting in an apoptosis-to-necrosis shift. *J. Biol. Chem.* **293**, 8032–8047 (2018).
76. Nukaya, M. *et al.* CDK7 is a Novel Therapeutic Vulnerability in Fibrolamellar Carcinoma. *bioRxiv* 2023.04.22.537934 (2023). doi:10.1101/2023.04.22.537934
77. Turnham, R. E. & Scott, J. D. Protein kinase A catalytic subunit isoform PRKACA; History,

function and physiology. *Gene* **577**, 101–108 (2016).
78. Setten, R. L., Rossi, J. J. & Han, S.-P. The current state and future directions of RNAi-based therapeutics. *Nat. Rev. Drug Discov.* **18**, 421–446 (2019).
79. Hu, B. *et al.* Therapeutic siRNA: state of the art. *Signal Transduct. Target. Ther.* **5**, (2020).
80. Torbenson, M. Fibrolamellar Carcinoma: 2012 Update. *Scientifica (Cairo).* **2012**, 1–15 (2012).
81. Craig, J. R., Peters, R. L., Edmondson, H. A. & Omata, M. Fibrolamellar carcinoma of the liver: A tumor of adolescents and young adults with distinctive clinico-pathologic features. *Cancer* **46**, 372–379 (1980).
82. Elguindy, M. M. *et al.* PUMILIO, but not RBMX, binding is required for regulation of genomic stability by noncoding RNA NORAD. *Elife* **8**, 1–16 (2019).
83. Oikawa, T. *et al.* Model of fibrolamellar hepatocellular carcinomas reveals striking enrichment in cancer stem cells. *Nat. Commun.* **6**, 1–17 (2015).
84. Moffat, J. *et al.* A Lentiviral RNAi Library for Human and Mouse Genes Applied to an Arrayed Viral High-Content Screen. *Cell* **124**, 1283–1298 (2006).
85. Beaucage, S. L. Solid-phase synthesis of siRNA oligonucleotides. *Curr. Opin. Drug Discov. Devel.* **11**, 203–216 (2008).
86. Muller, S., Wolf, J. & Ivanov, S. A. Current Strategies for the Synthesis of RNA. *Curr. Org. Synth.* **1**, 293–307 (2004).
87. Nair, J. K. *et al.* Multivalent N-acetylgalactosamine-conjugated siRNA localizes in hepatocytes and elicits robust RNAi-mediated gene silencing. *J. Am. Chem. Soc.* **136**, 16958–16961 (2014).
88. Brown, K. M. *et al.* Expanding RNAi therapeutics to extrahepatic tissues with lipophilic conjugates. *Nat. Biotechnol.* **40**, 1500–1508 (2022).
89. Soutschek, J. *et al.* Therapeutic silencing of an endogenous gene by systemic administration of modified siRNAs. *Nature* **432**, 173–178 (2004).
90. Akinc, A. *et al.* Targeted delivery of RNAi therapeutics with endogenous and exogenous ligand-based mechanisms. *Mol. Ther.* **18**, 1357–1364 (2010).